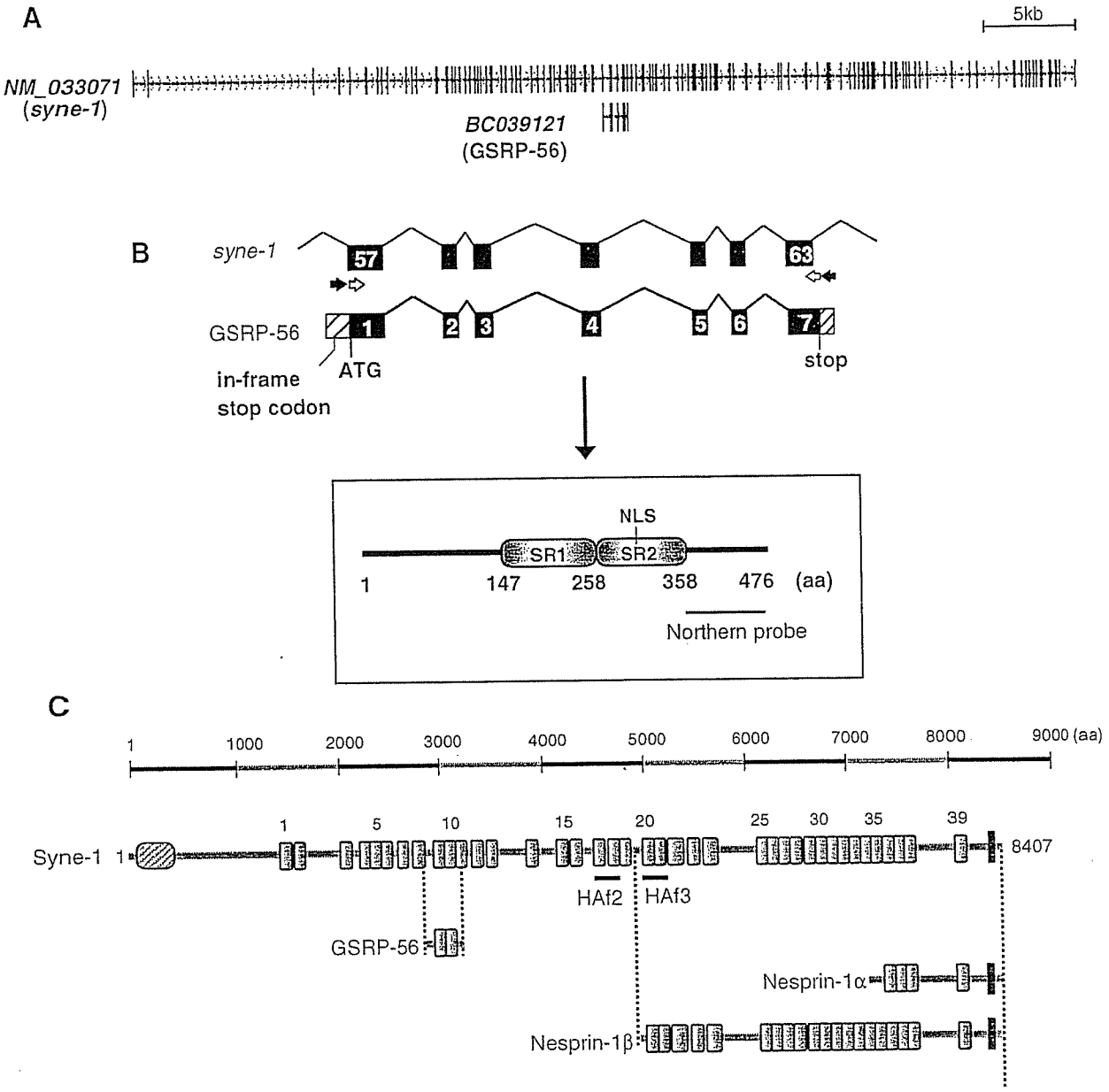

Fig. 1 – Schematic drawing of the gene structure of GSRP-56. (A) Genomic alignment of *syne-1* (GenBank accession no. *NM_033071*) and GSRP-56 (*BC039121*) using the UCSC BLAT program. Vertical lines indicate exons, whereas horizontal lines indicate introns. Small arrows on the vertical lines indicate direction of transcription. (B) Schematic drawings of the gene structures of *syne-1* and GSRP-56. The filled boxes represent exons, and the putative UTR is hatched. GSRP-56 is comprised of 7 exons, and its ORF begins at the position corresponding to exon 57 of *syne-1*. The black and white arrows indicate the region of primers used for PCR amplification of the region 5′-upstream of GSRP-56 (see Materials and methods). The lower panel shows the domain structure of GSRP-56 protein predicted by SMART. Tandem spectrin repeat motifs (SR) are shown. (C) Comparison of the predicted architectures of GSRP-56, longest Syne-1, and its two major splicing isoforms (Nesptin-1α and -1β). The N-terminal actin binding domain (ABD), SR domain, and the C-terminal transmembrane domain are denoted by a hatched box, shaded column, and vertical black bar, respectively. HAf2 and HAf3 represent positions of the proposed Golgi-binding sites of Syne-1 [28].

Northern and PCR analysis

An RNA blot from human multiple tissues (human MTN blot; BD Clontech) was probed with cDNAs labeled with ^{32}P using a random primed DNA labeling kit (Nippon Gene). The cDNA for β-actin (BD Clontech) was used as a positive control. Hybridization was performed at 68°C for 16 h using the ExpressHyb hybridization solution (BD Clontech) and ^{32}P-labeled RNA was visualized using a BAS imaging analyzer (FUJIFILM).

Plasmid construction and purification of recombinant proteins

All of the plasmids used in this study were produced by a PCR-based strategy. For plasmid construction of GST-, FLAG-, or GFP-tagged GSRP-56, PCR fragments corresponding to various regions of GSRP-56 were cloned into pGEX4T-1 expression vector (Amersham Pharmacia), p3xFLAG (Sigma), or pEGFP-C1 (BD Clontech), respectively. After expression of GST fusion proteins in *E. coli*, proteins were purified through glutathione sepharose 4B column (Pharmacia) according to the manufacturer's protocol.

Pull-down assay with GST fusion proteins

Ventricular tissues were taken from rats which were anesthetized according to the Guidelines for Animal Experimentation at the National Cardiovascular Center. Tissues were homogenized in PBS with 1% Triton X-100 by Physcotron (NITI-ON). The lysates were centrifuged and the resultant supernatant incubated with each GST fusion protein together with glutathione beads overnight at 4°C on a rotator. After washing four times with ice-cold PBS containing 0.5% Triton X-100, the bound proteins were eluted with 50 mM Tris–HCl solution containing 40 mM glutathione (pH 8.0) and subjected to SDS-PAGE followed by immunoblotting.

Immunoblotting and immunohistochemistry

Rat tissues and cultured cells were homogenized in RIPA lysis buffer. Extracts were separated on 10% SDS-polyacrylamide gels and transferred onto PVDF membranes (Millipore) as described previously [22]. The blots were visualized using a chemiluminescence detection system (Chemi-Lumi One; Nacalai Tesque) and signals were detected using an ECL-mini camera (Amersham Biosciences). For immunostaining of rat cardiomyocytes and other cultured cells, cells were fixed with 4% paraformaldehyde for 20 min at room temperature before permeabilization. After blocking with Blocking-One reagent (Nacalai Tesque), cells were incubated with primary antibodies diluted with blocking solution as follows: anti-S2, 1:200; anti-GM130, 1:250; anti-TGN38, 1:250; anti-nucleoporin-p62, 1:100; anti-Adaptin γ? 1:500. After washing, cells were incubated with biotin-conjugated goat anti-rabbit IgG secondary antibody (Zymed) diluted 1:500, followed by FITC-Streptavidin complex (Chemicon) diluted 1:1000 or rhodamine-conjugated donkey anti-mouse IgG secondary antibody (Chemicon) diluted 1:500. For antibody preabsorption, anti-S2 (1:100 diluted with PBS) solution was incubated with GST-GSRP-56 fusion protein (aa 1–358) at 4°C, overnight. Usually, aliquots of 10 μg of fusion proteins were added per 100 μl of solution. Fluorescence was observed using a confocal microscope (MRC 1024; Bio-Rad). Measurement of the area stained with anti-GM130 antibody was carried out using image analysis software (NIH Image version 1.63). GFP-negative and -positive cells on the same image were selected and subjected to data analysis.

Cell culture and plasmid transfection

Primary cardiomyocytes were isolated from the ventricles of fetal (embryonic day 21) rats and cultured as described previously [19]. Cardiomyocytes were maintained in M-199 medium (Sigma) supplemented with 10% fetal calf serum (FCS; Gibco) for 4 days before analysis. For immunohistochemical analysis, cells were usually grown on plastic dishes coated with collagen (Cellgen; Koken). C2C12 cells were grown in Dulbecco's modified Eagle's medium (DMEM; Sigma) supplemented with 5% FCS. Cells were grown to confluence, then transferred to differentiation medium containing 2% horse serum, and incubated for 3 days. HEK293 cells were grown in DMEM supplemented with 5% FCS. For transient transfection of plasmids, cells were grown on glass coverslips to 90% confluence and transfected using Lipofectamine 2000 reagent (Invitrogen) in the presence of serum in accordance with the manufacturer's protocol. Usually, 0.6 g of plasmid DNA and 2 μl of Lipofectamine reagent were used for cells on one coverslip. For FLAG-tagged proteins, aliquots of 6 μg of plasmids were transfected into cells in 60-mm dishes using 20 μl of Lipofectamine reagent. Six hours later, transfection medium was removed and cells were cultured with growth medium containing 5% FCS for 24–30 h.

Subcellular fractionation

Subcellular fractionation from rat heart muscles was carried out as described by Kapiloff et al. [23] with slight modifications. A rat heart was disrupted with Physcotron twice at 15,000 rpm for 15 s in 10 ml of Buffer B (10 mM HEPES pH 7.4, 5 mM EDTA, and protease inhibitors) with 0.32 M sucrose. The homogenate was filtered through a cell strainer with pores 100 μm in diameter and subjected to low-speed centrifugation at 3800×*g* for 20 min. The pellet (crude nuclear fraction) was resuspended in 10 ml of buffer B containing 2.4 M sucrose and further centrifuged at 50,000×*g* for 90 min, while the supernatant was centrifuged for 1 h at 100,000×*g*. The resultant pellets (nuclei and crude membrane fractions, respectively) were then resuspended in buffer B containing 0.32 M sucrose and subjected to SDS-PAGE followed by immunoblotting.

Results

Cloning and characterization of GSRP-56 cDNA

To identify the potential regulatory protein of TRPV2, we carried out a yeast two-hybrid screen using the N-terminal cytosolic domain of TRPV2 as bait. One of the positive clones grown on –H/A/L/T high stringency selection plates (see Materials and methods) isolated in the screen was predicted to encode a protein containing multiple SR motifs. By subsequent screening of a human heart cDNA library, we isolated a 1.6-kb cDNA clone that seemed to have the entire open reading frame. Using public EST database information, the sequence of this clone (named GSRP-56, Golgi-localized spectrin repeat-containing protein-56) was shown to be nearly identical to that of an EST clone deposited in GenBank (accession no. BC039121) as 'a partial mRNA of Syne-1' isolated from human testis by the NIH-MGC Project [24]. By genomic sequence search using UCSC BLAT, this clone was predicted to be an as yet unidentified form among

multiple splicing variants produced from the *syne-1* gene (Fig. 1A). The GSRP-56 cDNA is estimated to be produced from seven exons corresponding to exons 57–63 of the large *syne-1* gene with an unspliced intron between exons 63 and 64 (Fig. 1B). This unspliced intron contains a stop codon and subsequent polyadenylation signal sequence. To confirm whether this clone was a partial fragment, we searched for a cDNA clone with a longer 5′-UTR by PCR analysis using primers corresponding to the genomic 5′ upstream sequence and 3′-UTR sequence of GSRP-56, respectively (see Materials and methods). A 1.6 kb cDNA fragment including an in-frame termination codon 146 bases upstream of the first ATG was amplified. Therefore, we concluded that the original cDNA contained the complete ORF. The GSRP-56 cDNA was predicted to encode a protein of 476 aa. Using the SMART algorithm, we found that GSRP-56 contained two tandem SR motifs (Fig. 1B). The second SR contains a nuclear localization signal, although it is unclear whether this motif functions in cells. Fig. 1C shows a schematic drawings of the secondary structures of GSRP-56 and major Syne-1 isoforms reported to date.

Interaction of GSRP-56 with TRPV2

To determine the TRPV2-binding domain of GSRP-56, we purified recombinant GST fusion proteins containing various regions of GSRP-56. Lysate from rat heart was incubated with glutathione beads in the presence of these proteins. After washing and elution with glutathione, we checked the interaction of TRPV2 with these proteins by detecting TRPV2 in the eluted fractions by immunoblotting. We found that endogenous TRPV2 in rat heart bound to GST fusion proteins containing aa 1–358 of GSRP-56 (GST-1–358) as well as full-length GSRP-56 (GST-1–476) (Fig. 2A). TRPV2 also bound to the GSRP-56 protein lacking the second SR domain (aa 1–258), but its binding ability was slightly lower than those of GST-1–358 and GST-1–476. TRPV2 did not interact with GST itself or GST fusion proteins containing aa 1–147 (Fig. 2A). These results demonstrated that two SR domains are required for interaction of GSRP-56 with TRPV2 (Fig. 2B).

Tissue distribution of GSRP-56

Next, we analyzed the tissue distribution of GSRP-56. Northern blotting analysis revealed that the signal for GSRP-56 mRNA (approximately 1.6 kb) was detected predominantly in the human heart, whereas weak signals were detected in skeletal muscle, spleen, kidney, and lung (Fig. 3A). The size of this transcript agreed well with the length of isolated GSRP-56 cDNA. The 1.6-kb transcript seems to be a major product in heart and skeletal muscles, but various other transcripts of different sizes were also detected using our probe on Northern blotting. Subsequently, to evaluate the protein expression of GSRP-56, we prepared rabbit antiserum against the recombinant protein of the second SR region of GSRP-56 (referred to as anti-S2). To evaluate the reactivity of this antiserum, we prepared FLAG-tagged GSRP-56 expressed in HEK293 cells. Immunoblotting analysis demonstrated that anti-S2 strongly recognized the protein

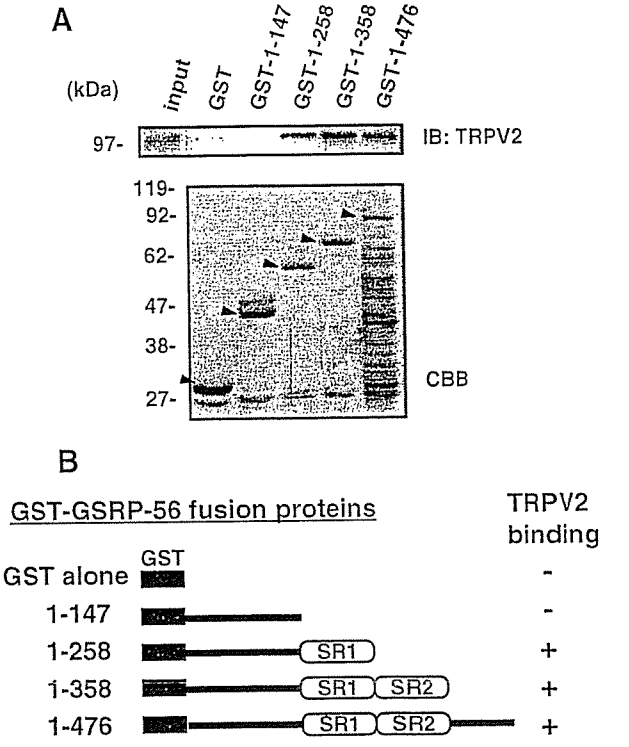

Fig. 2 – Pull-down assay for interaction of GSRP-56 with TRPV2. (A) GST fusion proteins containing various fragments of GSRP-56 were incubated with rat heart homogenate in the presence of glutathione-sepharose beads. After washing, bead-bound proteins were eluted with glutathione as described in Materials and methods. The eluted fractions were detected by immunoblotting analysis with anti-TRPV2 antibody (upper panel). Eluted proteins were stained with Coomassie Brilliant Blue (CBB) to detect the presence of GST fusion proteins (lower panel, arrowheads). (B) Schematic diagram of GST fusion protein constructs containing various regions of GSRP-56 to summarize their binding affinities to TRPV2.

with a molecular mass of 56 kDa, which was the same as that of the protein recognized by anti-FLAG antibody (Fig. 3B). This molecular mass was clearly coincident with that estimated from the primary structure of GSRP-56 (Fig. 3B).

As the 1.6-kb mRNA probably corresponding to GSRP-56 was detected predominantly in heart and skeletal muscles, we examined the protein expression pattern with anti-S2 in these tissues. As shown in Fig. 3C, anti-S2 recognized the 56-kDa protein band in both heart and skeletal muscles, but not in brain. Anti-S2 recognized an additional protein band of ~80 kDa in heart extracts. We considered that this 80-kDa protein band may correspond to another unidentified splicing variant of Syne-1 with the second SR region sequence of GSRP-56. The 56-kDa protein was also detected in the lysate of rat primary cardiomyocytes and mouse C2C12 muscle cells, but not in HEK293 cells with anti-S2 antibody (Fig. 3D). In contrast to the results of immunoblotting analysis of proteins from heart tissues, the 80-kDa band was not detected in cultured cardiomyocytes, although the reason for this observation is not yet clear.

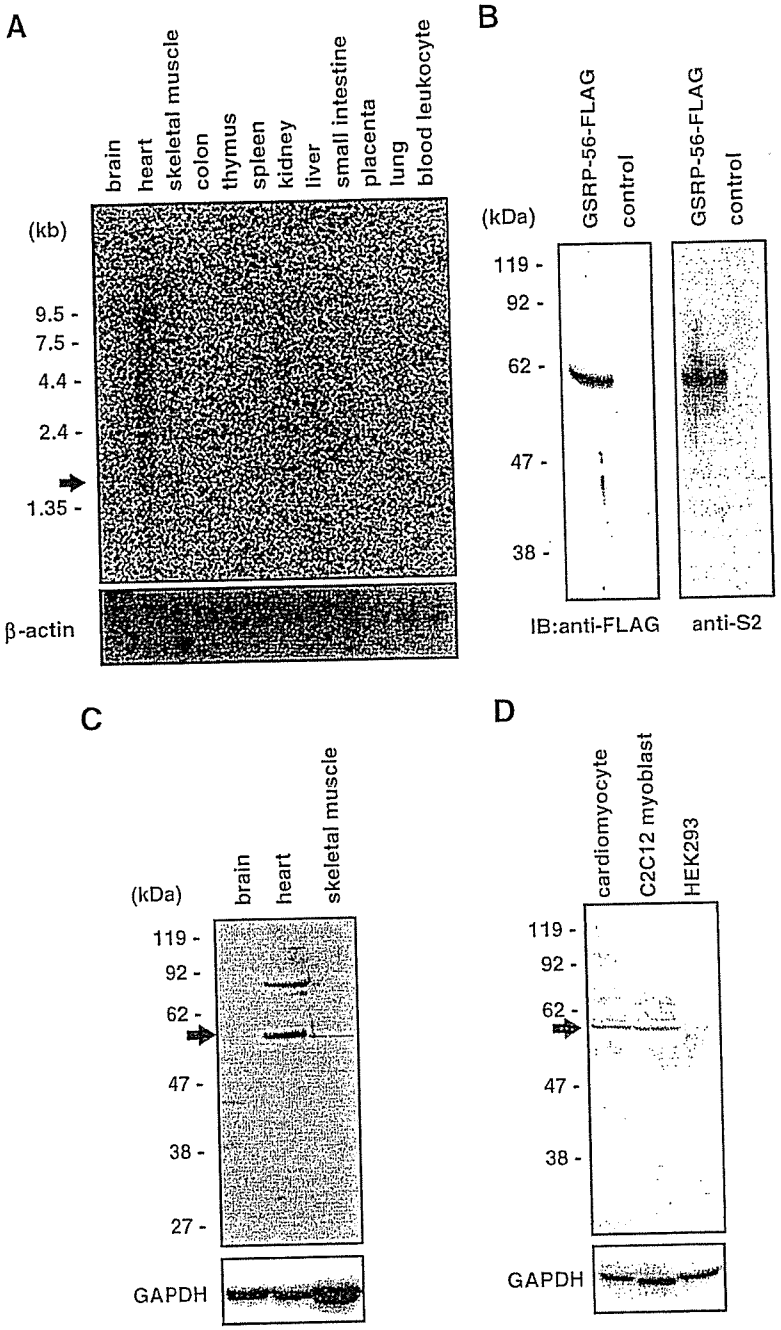

Fig. 3 – Tissue distribution of GSRP-56 transcript. (A) Northern blot of GSRP-56 in adult human tissues. The 1.6-kb GSRP-56 transcript (arrow) was detected predominantly in the heart. The region used as a probe is shown in Fig. 1B. A probe for β-actin was used to ensure equal loading of lanes. (B) Whole-cell extracts from HEK293 cells expressing FLAG-tagged full-length GSRP-56 or no-exogenous protein (control) were analyzed by immunoblotting using anti-FLAG (left panel) and anti-S2 (right panel) antibodies. Anti-FLAG antibody recognized a 56-kDa protein corresponding to the predicted molecular mass of GSRP-56. Anti-S2 antibody was shown to react specifically with the expressed protein. (C) Aliquots of 80 μg of rat tissue proteins were analyzed by immunoblotting with anti-S2 antibody. The antibody recognized 56-kDa protein (arrow). As a control experiment, half the amounts of proteins were analyzed with anti-GAPDH antibody (lower panel). (D) Immunoblotting for proteins from cultured cells. Rat primary cardiomyocytes, mouse C2C12 myoblast cells, and HEK293 cells were cultured and harvested, and homogenized proteins (50 μg) were subjected to immunoblotting analysis with anti-S2 antibody. The antibody recognized 56-kDa protein (arrow). As a control experiment, half the amounts of proteins were analyzed by immunoblotting with anti-GAPDH antibody (lower panel).

Golgi localization of GSRP-56

To analyze the subcellular localization of GSRP-56, we performed immunohistochemical analysis with anti-S2 antibody using rat primary cardiomyocytes and mouse C2C12 muscle cells. Anti-S2 antibody strongly labeled the perinuclear region of rat primary cardiomyocytes (Fig. 4A, a). The Golgi apparatus of cardiomyocytes was reported to be ring-shaped around the nucleus [25]. The staining pattern with antibody against GM130, cis-Golgi matrix protein (Fig. 4A, b) was consistent with these previous reports, and mostly overlapped with the distribution of anti-S2 staining (Fig. 4A, c), suggesting that GSRP-56 is localized predominantly in the Golgi apparatus of cardiomyocytes. As most Syne-1 isoforms have been shown to be localized at the nuclear membrane [9,10,12], which is often located close to the Golgi apparatus, we carried out subcellular fractionation of rat heart tissue to further analyze which organelles are associated with GSRP-56. According to the method described by Kapiloff et al. [23], rat heart homogenate was separated into nuclei and crude membrane fractions. The 56-kDa protein band was enriched in the membrane fraction where TRPV2 and the Golgi marker proteins GM130 and

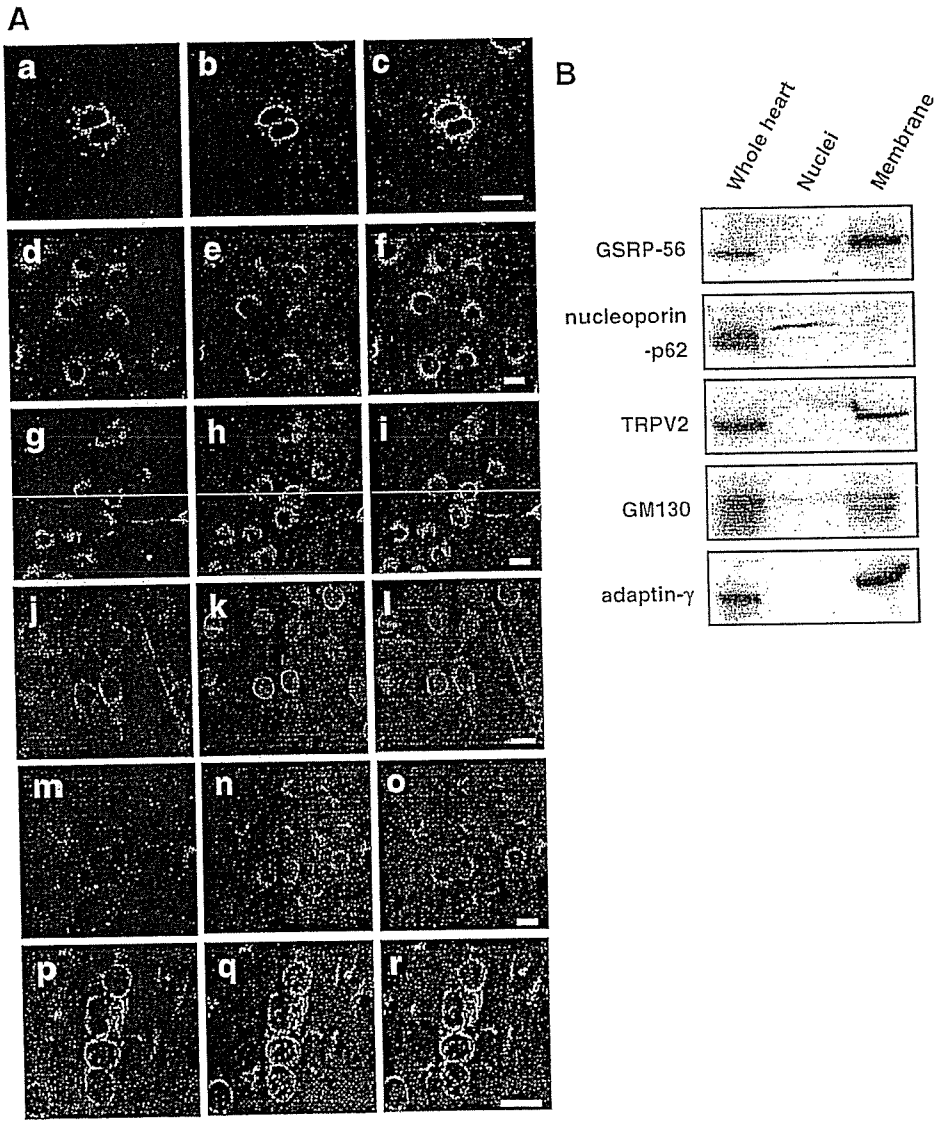

Fig. 4 – Subcellular localization of GSRP-56. (A) Rat primary cardiomyocytes (a–c), C2C12 myoblast cells (d–o), and C2C12 myotubes (3-day culture in differentiation medium, p–r) were double-stained with anti-S2 antibody (a, d, g, j, and p), the antibody for Golgi marker proteins, anti-GM130 (b, e, n, and q) or anti-TGN38 (h), and nuclear marker protein anti-nucleoporin-p62 (k). To test the specificity of antibody, antigen-preabsorbed anti-S2 was used in panel m. Panels c, f, i, l, o, and r show merged images. Scale bar=20 μm. (B) Subcellular fractionation analysis of adult rat heart. Rat heart homogenates were subjected to subcellular fractionation as described in Materials and methods. The crude membrane fraction contained sarcoplasmic reticulum, Golgi apparatus, and plasma membranes. Aliquots of 30 μg of proteins for each fraction were subjected to SDS-PAGE followed by immunoblotting analysis. A 56-kDa protein (GSRP-56) was detected by anti-S2 antibody. Antibodies against nucleoporin-p62 and TRPV2 served as markers for nucleus and membranes, respectively. Antibodies against GM130 and adaptin-γ were used as Golgi markers.

adaptin-γ were detected (Fig. 4B). However, the 56-kDa protein was not detected in nuclei where the nuclear marker nucleoporin-p62 was detected (Fig. 4B). These results suggest that GSRP-56 does not exist in the nucleus.

In C2C12 myoblast cells, anti-S2 antibody labeled distinct perinuclear structures (Fig. 4A, d). This polarized distribution pattern seemed to reflect that of the Golgi apparatus, because this structure was also recognized by the anti-GM130 (Fig. 4A, e). The merged image indicates that the polarized staining patterns with these antibodies overlapped at least partly (Fig. 4A, f). On the other hand, anti-S2 staining did not appear to overlap with that of anti-TGN38, a *trans*-Golgi marker protein (Fig. 4A, g–i) or a nuclear marker protein nucleoporin-p62 (Fig. 4A, j–l). As a negative control experiment, perinuclear labeling was confirmed to disappear when anti-S2 antibody was preabsorbed with the GSRP-56 antigen protein (Fig. 4A, m–o). These results suggest that GSRP-56 is a *cis*-Golgi-localized protein. To evaluate the changes in staining during muscle differentiation, we next performed immunocytochemical analysis in C2C12 myotubes 3 days after switching to differentiation medium (Fig. 4A, p–r). After differentiation, the staining pattern with anti-S2 antibody changed to a more dense ring-shaped distribution around the nucleus (Fig. 4A, p). This ring-shaped structure was well stained with anti-GM130 (Fig. 4A, q) as reported previously in differentiating myotubes [26,27]. These results suggest that GSRP-56 is localized at the Golgi apparatus in both C2C12 myoblasts and differentiated myotubes.

As an alternative approach to evaluate the Golgi localization of GSRP-56, we tested sensitivity to brefeldin A (BFA), a Golgi-destabilizing agent. Previous studies have demonstrated that the Golgi-specific spectrins associate with Golgi membranes in a BFA-sensitive manner [28–30]. Therefore, it was of interest to examine whether BFA treatment would disrupt the association of GSRP-56 with the Golgi complex, as in the case of these proteins. As shown in Fig. 5A, treatment of C2C12 myoblasts for 20 min with BFA resulted in disruption of the stacked Golgi structure as evidenced by staining with anti-adaptin-γ antibody (Fig. 5A, c). The same treatment also induced a rapid dispersion of anti-S2 staining (Fig. 5A, a). A similar effect was observed in C2C12 myotubes (data not shown). We next examined the effects of detergent treatment on GSRP-56 localization. Cells were treated with PBS containing 0.5% Triton X-100 for 10 min prior to fixation leading to the formation of a detergent insoluble structure—a 'Golgi ghost' [28,31]. Previous report have revealed that the Golgi-specific spectrin isoform was retained on tubular vesicular Golgi ghosts even after extraction [31]. The signal detected with anti-S2 antibody disappeared upon detergent treatment (Fig. 5B, a), despite preservation of the Golgi structure as evidenced by staining with anti-GM130 (Fig. 5B, c). These results indicate that GSRP-56 associates with the Golgi apparatus in a BFA-sensitive, but detergent-separable manner.

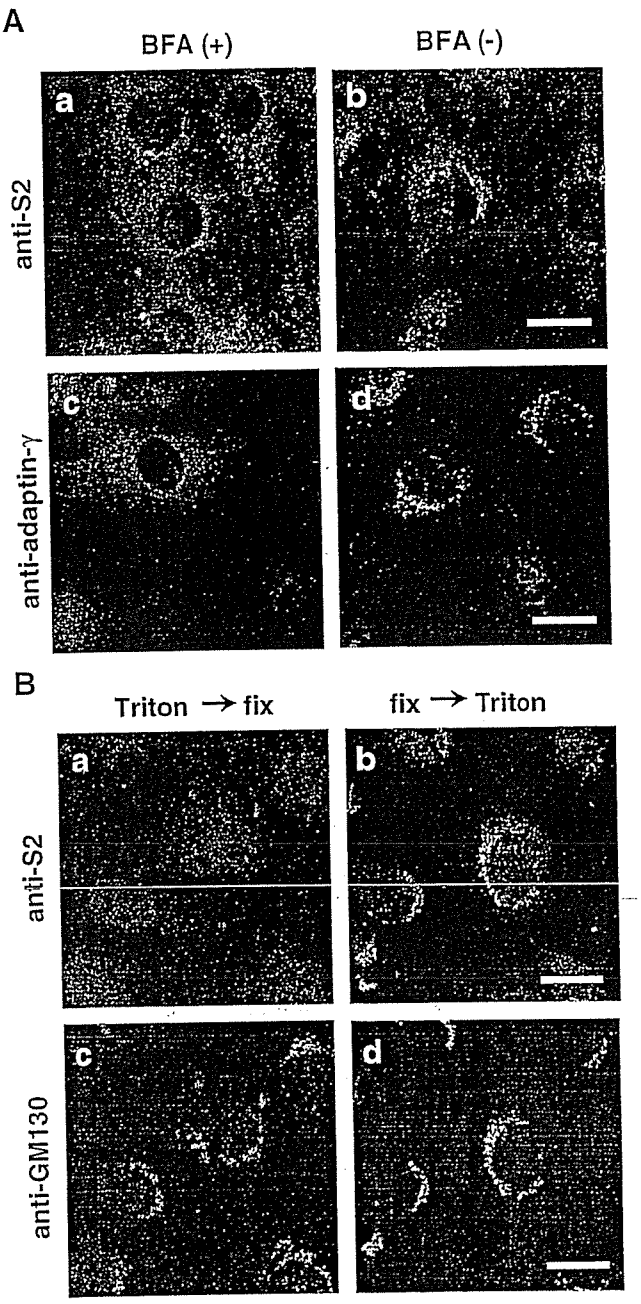

Fig. 5 – Effects of BFA and detergent treatment on Golgi localization of GSRP-56. (A) Effects of BFA. C2C12 myoblasts were treated with (a and c) or without (b and d) 50 μM BFA for 20 min at 37°C before fixation. Fixed cells were stained with anti-S2 antibodies (a and b) or anti-adaptin-γ (c and d). (B) C2C12 myoblasts were treated with 0.5% Triton X-100 for 10 min at room temperature either before (a and c) or after (b and d) fixation. Cells were stained with anti-S2 (a and b) or anti-GM130 antibody (c and d).

Golgi-targeting domain of GSRP-56

To determine the domain(s) that mediate the association of GSRP-56 with the Golgi apparatus, the expression vector carrying GFP-tagged GSRP-56 was transfected into HEK293 cells. The perinuclear concentrated GFP-signal was observed when full-length GSRP-56 (GFP-1–476) was expressed in HEK293 cells (Fig. 6A, a). This polarized localization at least partly overlapped with that of GM130 (Fig. 6A, b and c), further confirming that GFP-1–476 has the ability to target the Golgi in HEK293 cells. Subsequently, GFP-tagged deletion constructs were made and transfected into HEK293 cells. While deletion of the C-terminus (GFP-1–358, Fig. 6A, d–f) did not affect the

Golgi-localization of GSRP-56, deletion of two SR domains (GFP-1–147) completely inhibited the Golgi-localization (Fig. 6A, m, summarized in Fig. 6B). Deletion of the second SR domain (GFP-1–258) preserved the Golgi localization of GSRP-56, although most part of GSRP-56 was distributed in the cytosol (Fig. 6A, g–i). Similar localization patterns were observed in C2C12 myoblasts when GFP-tagged GSRP-56 variants were expressed (data not shown). Notably, a portion of GFP-tagged proteins containing only one or two SR domains were localized to the nucleus (Figs. 6A, j and n), probably due to the nuclear localization signal within the second SR domain. However, GFP-tagged protein with two SR domains (GFP-148–358) retained the ability to associate with the Golgi apparatus (Fig. 6A, j–l). These results suggest that both the first and second SR domains are required for effective targeting of GSRP-56 to the Golgi apparatus.

GSRP-56 changes morphology of the Golgi apparatus

We observed a change in morphology of the Golgi when GFP-tagged full-length GSRP-56 was expressed in HEK293 cells. Interestingly, the clearly enlarged, diffused Golgi structure was observed in GFP-positive cells by immunostaining with anti-GM130 (Fig. 7A, right panel arrowheads) but not GFP-negative non-transfected cells (Fig. 7A arrows). As shown in magnified images (Fig. 7A lower right panel), this enlargement was appeared to be partly derived from fragmentation of Golgi membranes. The area stained with anti-GM130 was measured and summarized in Fig. 7B. Expression of GSRP-56 increased the anti-GM130-stained area by approximately twofold, while expression of the deletion mutant GFP-1–147 lacking the Golgi localization signal had no effect (Fig. 7C, summarized in D), suggesting that GSRP-56 may regulate the morphology of the Golgi apparatus.

Discussion

In this study, we identified a novel SR-containing protein, GSRP-56, as a result of screening for TRPV2-interacting proteins. GSRP-56 is specified as a yet unidentified splicing isoform produced from a giant gene, *syne-1*, in a manner including an unspliced intron insertion. GSRP-56 shows two unique features that have not been reported in other splicing variants derived from *syne-1*. First, the transcript of this isoform is exceptionally small (1.6 kb) and is derived from a central region of the parental gene. Therefore, GSRP-56 protein does not contain any clear functional domains other than two SR domains, although most Syne-1 isoforms have a flanking N-terminal actin binding domain and/or C-terminal transmembrane domain, in addition to multiple SR domains. Thus, GSRP-56 is the rare example having only SR-domains, although CPG2 (candidate plasticity gene 2), a brain-specific Syne-1 isoform that was recently reported to have only SR domains and exert a specific function in the regulation of endocytosis [32], unlike conventional Syne-1 function and localization. Second, GSRP-56 was localized mostly to the Golgi membranes, in sharp contrast to several other splicing isoforms, such as Syne-1A, Nesprin-1α and myne-1, which were reported to be localized to NE [9,10,12]. Recently, Gough et al. [28] isolated a partial fragment of bovine Syne-1 (MDBK clone4) by expression screening performed with Golgi-specific β-spectrin antibody, and reported that Syne-1 is a candidate for Golgi-spectrin [28,33]. Based on the observations that the coding sequence of GSRP-56 does not overlap with that of MDBK clone4 and that GSRP-56 can easily be extracted by Triton X-100 in contrast to detergent-insoluble Golgi-spectrin, we consider that GSRP-56 is a distinct isoform of Golgi-localized Syne-1.

We found that GSRP-56 targets the Golgi apparatus through its tandem SR domains. As GSRP-56 has neither obvious membrane association domains, such as MAD1 and MAD2 of β-spectrins [30,34], nor transmembrane regions, we suppose that its localization is mediated by interactions with other Golgi-localized protein(s). SR-containing proteins including Syne-1 are known to form homo- or hetero-oligomers *via* their SR domains [16,35]. Indeed, by GST pull-down assay we obtained evidence that GSRP-56 interacts with βI-spectrin expressed in heart (data not shown). An A-kinase anchoring protein (mAKAP) has been reported to be targeted to NE via its three SR domains [36], and this targeting was recently reported to occur through the SR-SR interaction between mAKAP and Nesprin-1α in the NE [17]. Therefore, it is likely that GSRP-56 is localized to the Golgi apparatus through SR-mediated interaction with Golgi-specific cytoskeletal proteins. Gough et al. [15,28] proposed two Golgi binding regions of Syne-1, named HAf2 and HAf3. Interestingly, using SMART we found that HAf2 and HAf3 each contain two SRs (see Fig. 1C), similarly to GSRP-56.

In this study, we found that extensive enlargement of the Golgi apparatus occurred in HEK293 cells upon overexpression of GFP-tagged GSRP-56. The observed changes of the Golgi morphology may be caused by derangement of membrane integrity and/or defects in vesicular trafficking systems upon overexpression of GSRP-56. As distinct subtypes of spectrin (βI, βIII) and ankyrin (AnkG119, Ank195) were supposed to form a cytoskeletal meshwork and to function as a structural support of membrane organization [2,8], it is possible that expression of GSRP-56 affects the cytoskeletal organization. Gough et al. [28] reported that expression of the Golgi-binding fragment of Syne-1 (HAf3) in MDBK cells causes compaction of the Golgi apparatus, suggesting that expression of this domain exerts a dominant negative effect by competing with endogenous Syne-1. This apparently opposite effects of two Golgi-targeting polypeptides, GSRP-56 and HAf3, raises the interesting possibility that different SR domains maintain the structure of the

Fig. 6 – Identification of Golgi-targeting domain of GSRP-56. (A) Subcellular localization of GFP-tagged proteins including various regions of GSRP-56 (a–n) and GFP alone (o) in transiently transfected HEK293 cells. Typical expression patterns of each construct are shown. Samples were co-immunostained with anti-GM130 antibody (b, e, h, and k). Merged GFP fluorescence and GM130-stained images are shown in panels c, f, i, and l. Arrowheads and arrows indicate the overlapping or not-overlapping localization of GFP-GSRP-56 and anti-GM130 staining, respectively. Nuclei were labeled by 'N'. Scale bar=20 μm. (B) Schematic representation of GFP-GSRP-56 fusion constructs and summary of the subcellular localization.

A

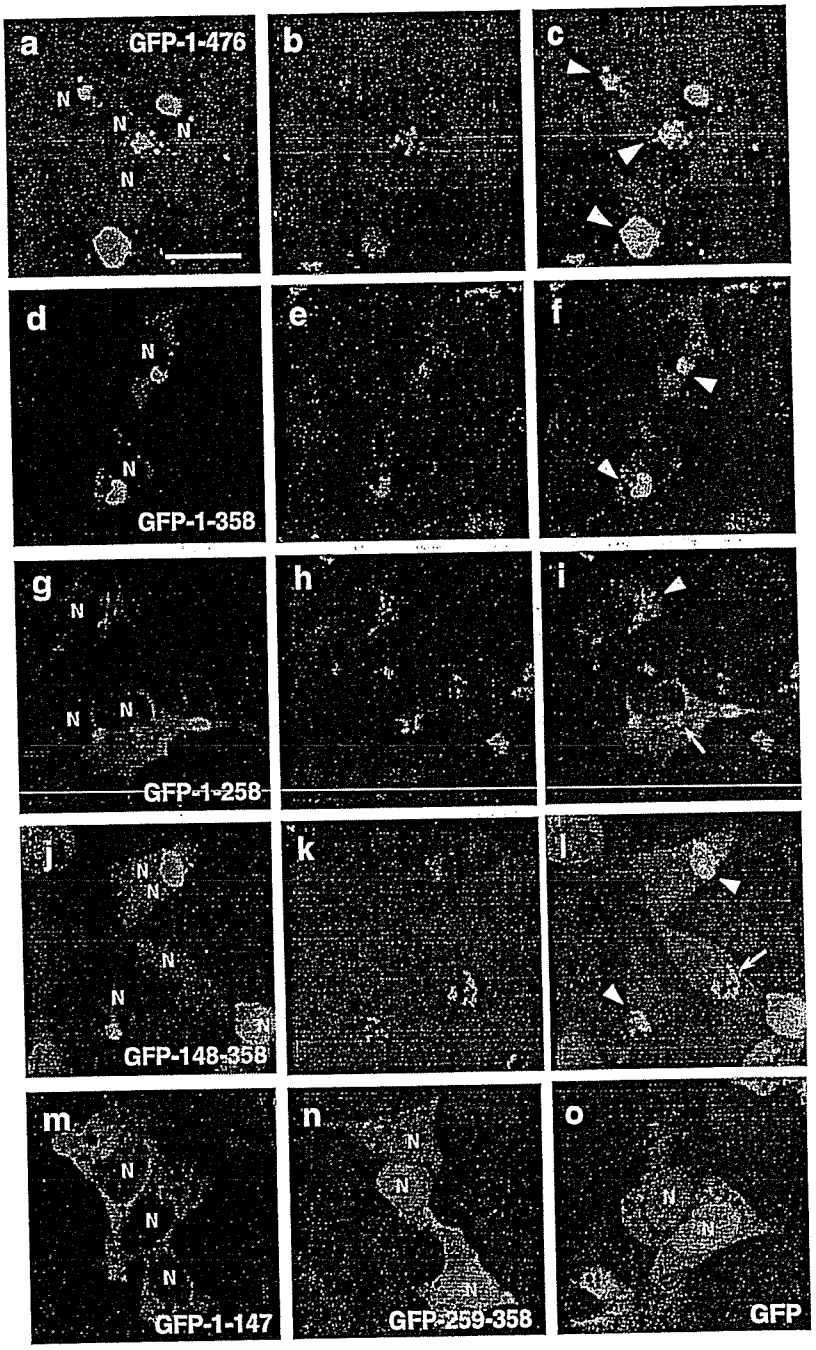
a
GFP-1-476
b
c
d
GFP-1-358
e
f
g
GFP-1-258
h
i
j
GFP-148-358
k
l
m
GFP-1-147
n
GFP-259-358
o
GFP
N

B

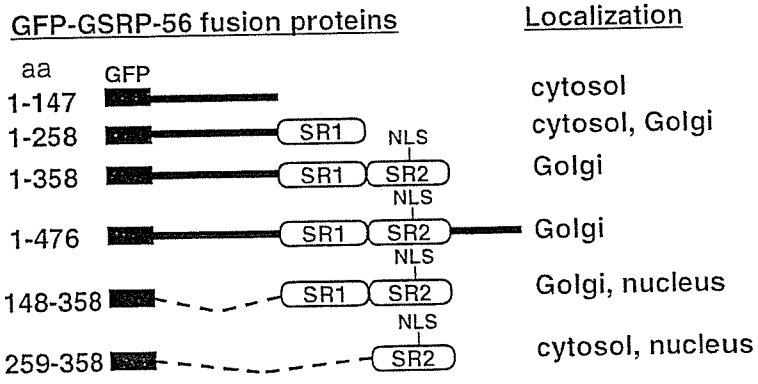
GFP-GSRP-56 fusion proteins
Localization
aa
GFP
1-147
cytosol
1-258
SR1
NLS
cytosol, Golgi
1-358
SR1
SR2
Golgi
NLS
1-476
SR1
SR2
Golgi
NLS
148-358
SR1
SR2
Golgi, nucleus
NLS
259-358
SR2
cytosol, nucleus

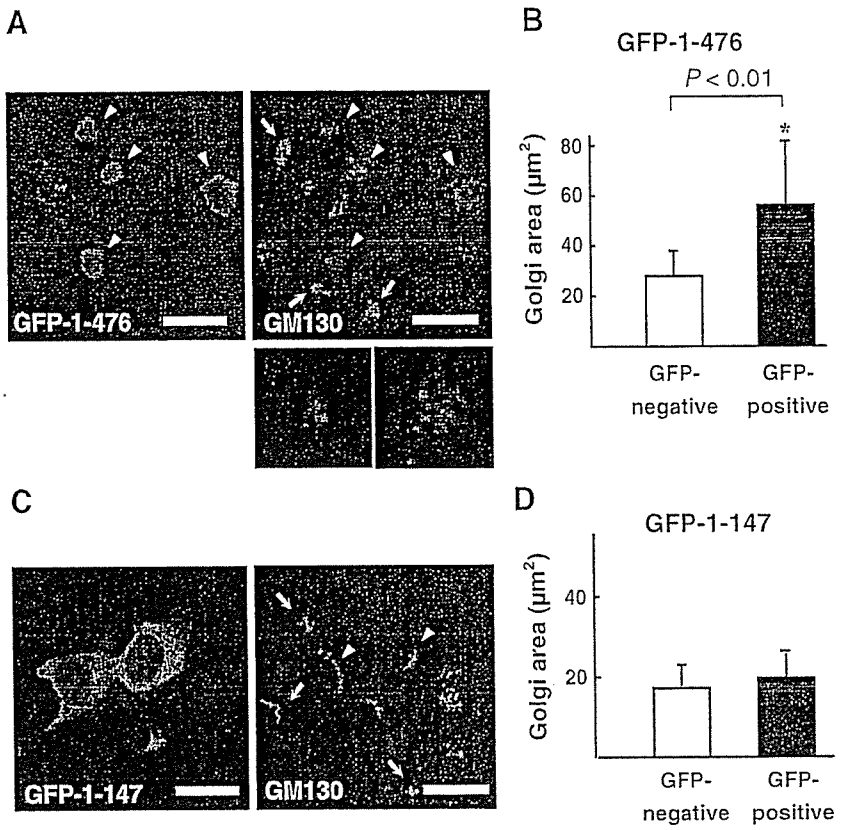

Fig. 7 – Effects of overexpression of GSRP-56 on the morphology of the Golgi apparatus. (A) Images of HEK293 cells transfected with GFP-tagged full-length GSRP-56 (GFP-1–476). GFP fluorescence (left) and staining pattern with anti-GM130 (right) are indicated. GFP-positive and -negative cells are marked by arrowheads and arrows, respectively. The Golgi apparatus of GFP-positive cells appeared to be more enlarged as compared to GFP-negative cells. Scale bar=20 μm. Lower panels show magnified images of typical staining pattern with anti-GM130 of a GFP-negative (left) or a GFP-positive (right) cell. (B) Comparison of anti-GM130 stained areas between GFP-positive and negative cells transfected with the full-length GSRP-56. Data are means±SD of 52 GFP-negative cells (*$P<0.01$ versus GFP-negative cells) and 16 GFP-positive cells, respectively. Mean values were 27.7 μm^2 for GFP-negative cells and 55.2 μm^2 for GFP-positive cells. (C) Images of HEK293 cells transfected with the deletion mutant GSRP-56 (GFP-1–147). GFP-fluorescence (left) and staining pattern with anti-GM130 (right) are indicated. (D) Comparison of GM130-stained areas between GFP-positive and -negative cells transfected with GFP-1–147. Data are means±SD of 20 GFP-negative cells and 17 GFP-positive cells, respectively. Mean values were 17.5 μm^2 for GFP-negative cells and 19.8 μm^2 for GFP-positive cells. The difference in mean value between GFP-negative cells in panels B and D may be due to the differences in experimental conditions of immunostaining.

Golgi apparatus by balancing dilation and compaction under physiological conditions.

Finally, it should be noted that GSRP-56 interacts with the TRPV2 channel. A murine TRPV2 (also referred to as GRC) is known to show regulated translocation from the intracellular compartment to the plasma membrane upon stimulation by growth factors in insulinoma cells [37], by neuropeptide head activator in neuroendocrine cells [38], and by membrane stretching in cultured myotubes [18]. Initially, we isolated GSRP-56 as a candidate for TRPV2 binding protein by a yeast two-hybrid screen. This is the first evidence for a direct interaction of the cytoskeletal element with this channel. However, despite extensive study using cultured cells and tissues, we have not yet confirmed the endogenous interaction between GSRP-56 and TRPV2 by co-immunoprecipitation or immunofluorescence analyses. It is possible that the physiological binding partner for TRPV2 may be the unidentified Syne-1 isoform(s) with larger size, which includes the GSRP-56 sequence. However, we confirmed that GSRP-56 fusion protein certainly had the ability to interact with TRPV2 by GST pull-down analysis. Therefore we suppose that the interaction between these two proteins may be too transient and/or relatively weak to detect *in vivo*. Recently, RGA (recombinase gene activator) was reported to associate with TRPV2 [39]. However, RGA was not co-localized with TRPV2 in the plasma membranes and was suggested to interact with TRPV2 during the biosynthesis and early trafficking of the channel [40]. It is possible that GSRP-56 also exerts such a function as a transient scaffold for TRPV2 or regulates the translocation of TRPV2 through the involvement of other unidentified proteins at the Golgi.

In summary, we identified a novel Golgi-localized isoform of Syne-1, GSRP-56, which is different from the many splicing isoforms of Syne-1 reported to date. We presented evidence that SR domains of GSRP-56 participate in Golgi localization and interaction with TRPV2 and that GSRP-56 possibly play a

role in regulating the membrane morphology of the Golgi apparatus. Clearly, GSRP-56 is a new member with relatively small size among the *syne*-1-derived splicing isoforms, which may exert important physiological functions.

Acknowledgments

This work was supported by the Program for Promotion of Fundamental Studies in Health Sciences of the National Institute of Biomedical Innovation (NIBIO), the Research Grants for Cardiovascular Diseases (17A-1) and for Nervous and Mental Disorders (17B-2) from the Ministry of Health, Labor, and Welfare, a Grant from the Japan Heart Foundation, and Grants-in-aid for Scientific Research on Priority Areas (13142210) and for Exploratory Research (17659241), and a Grant for the Cooperative Link of Unique Science and Technology for Economy Revitalization from Ministry of Education, Science, and Culture of Japan.

REFERENCES

[1] V. Bennett, A.J. Baines, Spectrin and ankyrin-based pathways: metazoan inventions for integrating cells into tissues, Physiol. Rev. 81 (2001) 1353–1392.
[2] M.A. DeMatteis, J.S. Morrow, Spectrin tethers and mesh in the biosynthetic pathway, J. Cell Sci. 113 (Pt 13) (2000) 2331–2343.
[3] J. Pascual, J. Castresana, M. Saraste, Evolution of the spectrin repeat, BioEssays 19 (1997) 811–817.
[4] Y. Yan, E. Winograd, A. Viel, T. Cronin, S.C. Harrison, D. Branton, Crystal structure of the repetitive segments of spectrin, Science 262 (1993) 2027–2030.
[5] K. Djinovic-Carugo, M. Gautel, J. Ylanne, P. Young, The spectrin repeat: a structural platform for cytoskeletal protein assemblies, FEBS Lett. 513 (2002) 119–123.
[6] K.A. Beck, W.J. Nelson, The spectrin-based membrane skeleton as a membrane protein-sorting machine, Am. J. Physiol. 270 (1996) C1263–C1270.
[7] P. Devarajan, P.R. Stabach, A.S. Mann, T. Ardito, M. Kashgarian, J.S. Morrow, Identification of a small cytoplasmic ankyrin (AnkG119) in the kidney and muscle that binds beta I sigma spectrin and associates with the Golgi apparatus, J. Cell Biol. 133 (1996) 819–830.
[8] K.A. Beck, W.J. Nelson, A spectrin membrane skeleton of the Golgi complex, Biochim. Biophys. Acta 1404 (1998) 153–160.
[9] E.D. Apel, R.M. Lewis, R.M. Grady, J.R. Sanes, Syne-1, a dystrophin- and Klarsicht-related protein associated with synaptic nuclei at the neuromuscular junction, J. Biol. Chem. 275 (2000) 31986–31995.
[10] Q. Zhang, J.N. Skepper, F. Yang, J.D. Davies, L. Hegyi, R.G. Roberts, P.L. Weissberg, J.A. Ellis, C.M. Shanahan, Nesprins: a novel family of spectrin-repeat-containing proteins that localize to the nuclear membrane in multiple tissues, J. Cell Sci. 114 (2001) 4485–4498.
[11] V.C. Padmakumar, S. Abraham, S. Braune, A.A. Noegel, B. Tunggal, I. Karakesisoglou, E. Korenbaum, Enaptin, a giant actin-binding protein, is an element of the nuclear membrane and the actin cytoskeleton, Exp. Cell Res. 295 (2004) 330–339.
[12] J.M. Mislow, M.S. Kim, D.B. Davis, E.M. McNally, Myne-1, a spectrin repeat transmembrane protein of the myocyte inner nuclear membrane, interacts with lamin A/C, J. Cell Sci. 115 (2002) 61–70.
[13] R.M. Grady, D.A. Starr, G.L. Ackerman, J.R. Sanes, M. Han, Syne proteins anchor muscle nuclei at the neuromuscular junction, Proc. Natl. Acad. Sci. U. S. A. 102 (2005) 4359–4364.
[14] J. Fan, K.A. Beck, A role for the spectrin superfamily member Syne-1 and kinesin II in cytokinesis, J. Cell Sci. 117 (2004) 619–629.
[15] L.L. Gough, K.A. Beck, The spectrin family member Syne-1 functions in retrograde transport from Golgi to ER, Biochim. Biophys. Acta 1693 (2004) 29–36.
[16] J.M. Mislow, J.M. Holaska, M.S. Kim, K.K. Lee, M. Segura-Totten, K.L. Wilson, E.M. McNally, Nesprin-1alpha self-associates and binds directly to emerin and lamin A in vitro, FEBS Lett. 525 (2002) 135–140.
[17] G.C. Pare, J.L. Easlick, J.M. Mislow, E.M. McNally, M.S. Kapiloff, Nesprin-1alpha contributes to the targeting of mAKAP to the cardiac myocyte nuclear envelope, Exp. Cell Res. 303 (2005) 388–399.
[18] Y. Iwata, Y. Katanosaka, Y. Arai, K. Komamura, K. Miyatake, M. Shigekawa, A novel mechanism of myocyte degeneration involving the Ca^{2+}-permeable growth factor-regulated channel, J. Cell Biol. 161 (2003) 957–967.
[19] Y. Katanosaka, Y. Iwata, Y. Kobayashi, F. Shibasaki, S. Wakabayashi, M. Shigekawa, Calcineurin inhibits Na^+/Ca^{2+} exchange in phenylephrine-treated hypertrophic cardiomyocytes, J. Biol. Chem. 280 (2005) 5764–5772.
[20] W.J. Kent, BLAT-the BLAST-like alignment tool, Genome Res. 12 (2002) 656–664.
[21] J. Schultz, F. Milpetz, P. Bork, C.P. Ponting, SMART, a simple modular architecture research tool: identification of signaling domains, Proc. Natl. Acad Sci. U. S. A. 95 (1998) 5857–5864.
[22] Y. Iwata, H. Nakamura, Y. Mizuno, M. Yoshida, E. Ozawa, M. Shigekawa, Defective association of dystrophin with sarcolemmal glycoproteins in the cardiomyopathic hamster heart, FEBS Lett. 329 (1993) 227–231.
[23] M.S. Kapiloff, N. Jackson, N. Airhart, mAKAP and the ryanodine receptor are part of a multi-component signaling complex on the cardiomyocyte nuclear envelope, J. Cell Sci. 114 (2001) 3167–3176.
[24] R.L. Strausberg, et al., Generation and initial analysis of more than 15,000 full-length human and mouse cDNA sequences, Proc. Natl. Acad Sci. U. S. A. 99 (2002) 16899–16903.
[25] P.J. Kronebusch, S.J. Singer, The microtubule-organizing complex and the Golgi apparatus are co-localized around the entire nuclear envelope of interphase cardiac myocytes J. Cell Sci. 88 (Pt 1) (1987) 25–34.
[26] A.M. Tassin, M. Paintrand, E.G. Berger, M. Bornens, The Golgi apparatus remains associated with microtubule organizing centers during myogenesis, J. Cell Biol. 101 (1985) 630–638.
[27] Z. Lu, D. Joseph, E. Bugnard, K.J. Zaal, E. Ralston, Golgi complex reorganization during muscle differentiation: visualization in living cells and mechanism, Mol. Biol. Cell 12 (2001) 795–808.
[28] L.L. Gough, J. Fan, S. Chu, S. Winnick, K.A. Beck, Golgi localization of Syne-1, Mol. Biol. Cell 14 (2003) 2410–2424.
[29] K.A. Beck, J.A. Buchanan, V. Malhotra, W.J. Nelson, Golgi spectrin: identification of an erythroid beta-spectrin homolog associated with the Golgi complex, J. Cell Biol. 127 (1994) 707–723.
[30] A. Godi, I. Santone, P. Pertile, P. Devarajan, P.R. Stabach, J.S. Morrow, G. DiTullio, R. Polishchuk, T.C. Petrucci, A. Luini, M.A. DeMatteis, ADP ribosylation factor regulates spectrin binding to the Golgi complex, Proc. Natl. Acad Sci. U. S. A. 95 (1998) 8607–8612.
[31] K.A. Beck, J.A. Buchanan, W.J. Nelson, Golgi membrane skeleton: identification, localization and oligomerization of a 195 kDa ankyrin isoform associated with the Golgi complex, J. Cell Sci. 110 (Pt 10) (1997) 1239–1249.

[32] J.R. Cottrell, E. Borok, T.L. Horvath, E. Nedivi, CPG2: a brain- and synapse-specific protein that regulates the endocytosis of glutamate receptors, Neuron 44 (2004) 677–690.
[33] K.A. Beck, Spectrins and the Golgi, Biochim. Biophys. Acta 1744 (2005) 374–382.
[34] C.R. Lombardo, S.A. Weed, S.P. Kennedy, B. Forget, G. Morrow, Beta II-spectrin (fodrin) and beta I epsilon 2-spectrin (muscle) contain NH2- and COOH-terminal membrane association domains (MAD1 and MAD2), J. Biol. Chem. 269 (1994) 29212–29219.
[35] S.P. Kennedy, S.A. Weed, B.G. Forget, J.S. Morrow, A partial structural repeat forms the heterodimer self-association site of all beta-spectrins, J. Biol. Chem. 269 (1994) 11400–11448.
[36] M.S. Kapiloff, R.V. Schillace, A.M. Westphal, J.D. Scott, mAKAP: an A-kinase anchoring protein targeted to the nuclear membrane of differentiated myocytes, J. Cell Sci. 112 (Pt 16) (1999) 2725–2736.
[37] M. Kanzaki, Y.Q. Zhang, H. Mashima, L. Li, H. Shibata, I. Kojima, Translocation of a calcium-permeable cation channel induced by insulin-like growth factor-I, Nat. Cell Biol. 1 (1999) 165–170.
[38] K. Boels, G. Glassmeier, D. Herrmann, I.B. Riedel, W. Hampe, I. Kojima, J.R. Schwarz, H.C. Schaller, The neuropeptide head activator induces activation and translocation of the growth-factor-regulated Ca(2+)-permeable channel GRC, J. Cell Sci. 114 (2001) 3599–3606.
[39] J.C. Barnhill, A.J. Stokes, M. Koblan-Huberson, L.M. Shimoda, A. Muraguchi, C.N. Adra, H. Turner, RGA protein associates with a TRPV ion channel during biosynthesis and trafficking, J. Cell. Biochem. 91 (2004) 808–820.
[40] A.J. Stokes, C. Wakano, K.A. DelCarmen, M. Koblan-Huberson, H. Turner, Formation of a physiological complex between TRPV2 and RGA protein promotes cell surface expression of TRPV2, J. Cell. Biochem. 94 (2005) 669–683.

Novel role of neuronal Ca^{2+} sensor-1 as a survival factor up-regulated in injured neurons

Tomoe Y. Nakamura,[1,2] Andreas Jeromin,[4] George Smith,[5] Hideaki Kurushima,[3] Hitoshi Koga,[2] Yusaku Nakabeppu,[3] Shigeo Wakabayashi,[1] and Junichi Nabekura[2,6,7]

[1]Department of Molecular Physiology, National Cardiovascular Center Research Institute, Suita, Osaka 565-8565, Japan
[2]Department of Cellular and System Physiology, Graduate School of Medical Sciences and [3]Division of Neurofunctional Genomics, Department of Immunobiology and Neuroscience, Medical Institute of Bioregulation, Kyushu University, Fukuoka 812-8582, Japan
[4]Neuroscience, Baylor College of Medicine, Houston, TX 77030
[5]Department of Physiology, University of Kentucky Medical School, Lexington, KY 50536
[6]Division of Homeostatic Development, National Institute of Physiological Sciences, Okazaki 444-8585, Japan
[7]Core Research for Evolutional Science and Technology, the Japan Science and Technology Agency, Kawaguchi, Saitama 332-0012, Japan

A molecular basis of survival from neuronal injury is essential for the development of therapeutic strategy to remedy neurodegenerative disorders. In this study, we demonstrate that an EF-hand Ca^{2+}-binding protein neuronal Ca^{2+} sensor-1 (NCS-1), one of the key proteins for various neuronal functions, also acts as an important survival factor. Overexpression of NCS-1 rendered cultured neurons more tolerant to cell death caused by several kinds of stressors, whereas the dominant-negative mutant (E120Q) accelerated it. In addition, NCS-1 proteins increased upon treatment with glial cell line–derived neurotrophic factor (GDNF) and mediated GDNF survival signal in an Akt (but not MAPK)-dependent manner. Furthermore, NCS-1 is significantly up-regulated in response to axotomy-induced injury in the dorsal motor nucleus of the vagus neurons of adult rats in vivo, and adenoviral overexpression of E120Q resulted in a significant loss of surviving neurons, suggesting that NCS-1 is involved in an antiapoptotic mechanism in adult motor neurons. We propose that NCS-1 is a novel survival-promoting factor up-regulated in injured neurons that mediates the GDNF survival signal via the phosphatidylinositol 3-kinase–Akt pathway.

Introduction

Neuronal apoptosis is induced by numerous stressors and underlies many human neurodegenerative disorders, such as Alzheimer's and Parkinson's disease. Under such apoptotic conditions, several neurotrophic factors such as glial cell line–derived neurotrophic factor (GDNF) and brain-derived neurotrophic factor (BDNF) can activate the antiapoptotic process to rescue neurons from death. However, the signaling pathway leading to cell survival is not yet completely understood. GDNF was reported to exert a potent survival-promoting activity in neurons (Henderson et al., 1994; Oppenheim et al., 1995; Yan et al., 1995) and to reduce neuronal death induced by various toxic challenges both in vitro (Nicole et al., 2001) and in vivo (Wang et al., 2002; Kirik et al., 2004). Recent evidence suggests that a part of molecular mechanisms for GDNF-induced cell survival relates to an increase in intracellular Ca^{2+} concentration, and it subsequently activates some survival pathways such as the phosphatidylinositol 3-kinase (PI3-K)–Akt pathway (Perez-Garcia et al., 2004).

Ca^{2+} is the most versatile and important intracellular messenger in neurons, regulating a variety of neuronal processes such as neurotransmission and signal transductions. The various actions of Ca^{2+} are mediated by a large family of EF-hand Ca^{2+}-binding proteins, which may act as Ca^{2+} sensors or Ca^{2+} buffers. One of them, neuronal Ca^{2+} sensor-1 (NCS-1; mammalian homologue of frequenin), was originally identified in *Drosophila melanogaster* in a screen for neuronal hyperexcitability mutants (Mallart et al., 1991). Overexpression of NCS-1 has been shown to enhance evoked neurotransmitter release and exocytosis (Pongs et al., 1993; Olafsson et al., 1995). NCS-1 directly interacts with phosphatidylinositol 4-hydroxykinase (PI4-K; Hendricks et al., 1999; Weisz et al., 2000) and enhances neuronal secretion by modulating vesicular trafficking steps in

Correspondence to Tomoe Y. Nakamura: tomoen@ri.ncvc.go.jp

Abbreviations used in this paper: BDNF, brain-derived neurotrophic factor; DMV, dorsal motor nucleus of the vagus; GAPDH, glyceraldehyde-3-phosphate dehydrogenase; GDNF, glial cell line–derived neurotrophic factor; MEK, MAPK kinase; NCS-1, neuronal Ca^{2+} sensor-1; PH, pleckstrin homology; PI3-K, phosphatidylinositol 3-kinase; PI4-K, phosphatidylinositol 4-hydroxykinase.

The Journal of Cell Biology, Vol. 172, No. 7, March 27, 2006 1081–1091
http://www.jcb.org/cgi/doi/10.1083/jcb.200508156

a phosphoinositide-dependent manner (Koizumi et al., 2002). We have previously demonstrated that NCS-1 modulates the voltage-gated K^+ channel Kv4 (Nakamura et al., 2001). Subsequently, certain voltage-gated Ca^{2+} channels have also been reported to be regulated by NCS-1 (Weiss et al., 2000; Wang et al., 2001; Tsujimoto et al., 2002). Furthermore, NCS-1 enhances the number of functional synapses (Chen et al., 2001), potentiates paired pulse facilitation (Sippy et al., 2003), and may be involved in associative learning and memory in *Caenorhabditis elegans* (Gomez et al., 2001). Despite the participation of NCS-1 in a wide range of biological functions, however, the role of NCS-1 in neuronal survival under pathophysiological conditions or the involvement of NCS-1 in neurotrophic factor–mediated neuroprotection are unknown.

Because we found that the expression levels of NCS-1 is significantly higher in immature brain (Nakamura et al., 2003) and a remarkable similarity exists between immature and injured neurons during the development and regeneration process, respectively (Nabekura et al., 2002b), these findings prompted us to study the expression level and the functional roles of NCS-1 in damaged neurons.

In this study, we found that NCS-1 is a survival-promoting factor, which increases the resistance of neurons to several kinds of stressors. In addition, NCS-1 is up-regulated in response to axonal injury in adult motor neurons, and this protects cells from apoptosis. Furthermore, NCS-1 mediates GDNF-induced neuroprotection via activation of Akt pathways. This is the first study demonstrating a novel role of NCS-1 on neuronal survival.

Results

The expression level of NCS-1 protein increases with neuronal injury

To examine the expression level of NCS-1 in injured neurons, we performed unilateral vagal axotomy (transaction of nerves) on adult rats. 1 d to 2 mo after the in vivo axotomy, brainstems, including the bilateral dorsal motor nucleus of the vagus (DMV) neurons, were isolated. Immunohistochemical staining and computerized image analysis of frozen sections revealed that axotomy significantly (more than threefold) increased the expression level of NCS-1 in the DMV when compared with those on the control side at 1 wk after the surgery (Fig. 1, A–C). NCS-1 immunoreactivity was mainly expressed in cell bodies of neurons, as shown using hematoxylin counterstaining to identify the nuclei (Fig. 1 B, brown staining accompanied with blue staining; depicted by arrows). The increase in NCS-1 level started at 1 d after axotomy, reached a peak at 1 wk, and gradually decreased to control levels over the next 2 mo (Fig. 1 D). We also conducted quantitative immunoblot analysis on tissue samples from DMV neurons 1 d and 1 wk after axotomy, expressing NCS-1 density relative to levels of glyceraldehyde-3-phosphate dehydrogenase (GAPDH). The results confirmed the immunohistochemistry experiments, with levels of NCS-1 protein in ipsilateral DMV being increased significantly (by about threefold) by 1 wk after axotomy (Fig. 1, E and F).

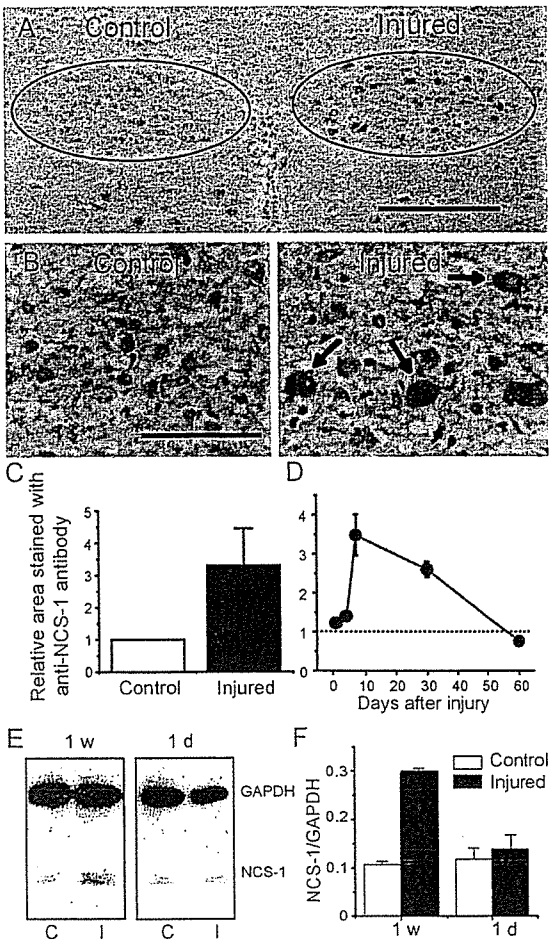

Figure 1. **NCS-1 is up-regulated in the DMV neurons after in vivo axotomy.** The 10th cranial nerve on one side of the neck of adult (4–6-wk-old) rats was cut, and, 1 d to 2 mo later, the brainstem was excised and frozen sections were cut. The NCS-1 expression was examined by counterstaining with NCS-1 antibody (brown signal) and with hematoxylin to identify nuclei (blue signal). (A) Staining pattern 1 wk after in vivo axotomy. The amount of NCS-1 protein increased in the DMV neurons ipsilateral to axotomy (injured side) when compared with control neurons contralateral to axotomy. Positions of DMV neurons are represented by circles. (B) Magnified image of DMV neurons. Arrows indicate that some neurons have both NCS-1 and hematoxylin staining, indicating that NCS-1 is expressed in cell bodies. Bars (A), 200 μm; (B) 50 μm. (C) Summarized data obtained by computerized image analysis. The relative area stained using NCS-1 antibody on the injured side 1 wk after axotomy was normalized to that of the control side (means ± SEM [error bars]; $n = 6$). (D) Time course of the expression levels of NCS-1 in injured DMV neurons relative to uninjured DMV neurons. Immunohistochemical analysis of NCS-1 levels were performed in rats 1, 4, 7, 30, and 60 d after axotomy (means ± SEM; $n = 6$). (E) Immunoblots indicating the expression levels of NCS-1 in the tissue samples obtained from DMV regions in brainstem sections at control (C) and injured sites (I) 1 wk and 1 d after axotomy. 10 sections were used for each group. Similar amount of proteins were loaded on the gel as indicated by the similar amount of the internal control GAPDH. (F) The densities of NCS-1 bands were expressed relative to the density of GAPDH bands in each tissue sample, and the group data is summarized (means ± SEM; $n = 3$).

Up-regulation of NCS-1 protein was also observed using a different type of stressor. Continuous treatment of neurons with colchicine for 4 d, which disrupts tubulin polymerization and blocks axonal transport, also increased NCS-1 expression levels (1.40 ± 0.03-fold above control levels; $P < 0.05$; $n = 4$), indicating that NCS-1 is up-regulated in vivo in response to two

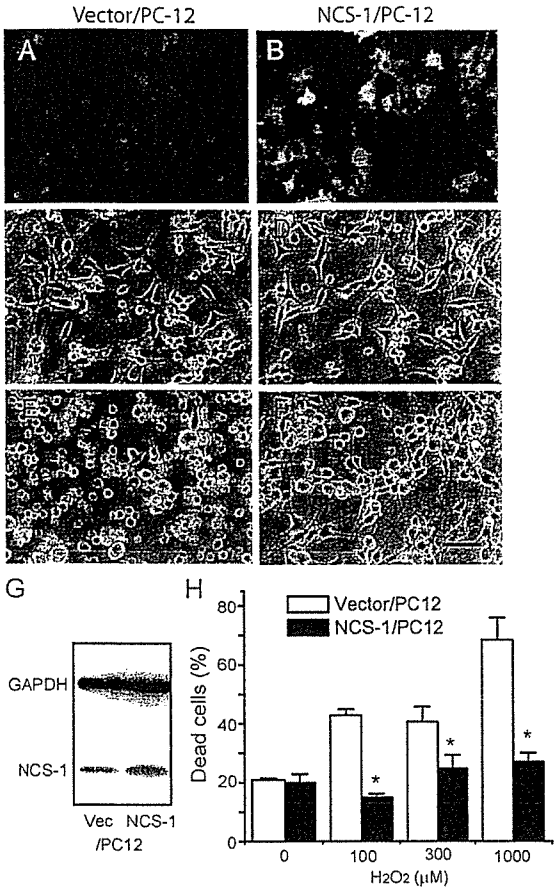

Figure 2. **Effects of the overexpression of NCS-1 on the susceptibility of PC-12 cells to H_2O_2 toxicity.** PC-12 cells stably transfected with NCS-1 (NCS-1/PC12) or vector alone (vector/PC-12) were differentiated into neuronlike cells by treatment with 100 ng/ml NGF and exposed to several concentrations (0–1 mM) of H_2O_2. (A and B) Immunofluorescent micrographs show that the expression level of NCS-1/PC12 cells is much higher than that in vector/PC12 cells. (C–F) Phase-contrast micrographs of PC-12 cells exposed to 0 (C and D) or 300 μM H_2O_2 for 3 d (E and F). Bar, 40 μm. (G) Representative immunoblots showing expression levels of NCS-1 in control vector and NCS-1–transfected cells. Also shown is the expression levels of the control protein GADPH obtained from immunoblots from the same cell samples. Unlike for NCS-1 levels, GADPH levels were not markedly different in control and NCS-1–transfected cells. (H) Bar graph shows the cell viability evaluated by trypan blue exclusion assay (means ± SEM [error bars]; $n = 8$). *, $P < 0.05$ versus vector/PC-12 cells.

different kinds of stressors—one being mechanical and the other being chemical injury.

Expression of NCS-1 renders PC-12 cells more tolerant to stressors

To study the physiological role of NCS-1 in damaged neurons, we next examined the effect of NCS-1 overexpression on the susceptibility of cells to several kinds of stressors. PC-12 cells stably transfected with either the NCS-1 expression vector (NCS-1/PC-12) or the vector alone (vector/PC-12) were differentiated into neuronlike cells, and the resistance to H_2O_2 toxicity was compared between these two groups. As shown in the immunofluorescent micrographs and immunoblot in Fig. 2 (A, B, and G), the expression level of NCS-1 was found to be significantly higher in NCS-1/PC-12 cells compared with vector-transfected cells, although these cells also had some endogenous NCS-1. Treatment with a relatively high dose (300 μM) of H_2O_2 for 3 d in the absence of pyruvate resulted in severe cellular damage in vector/PC-12 control cells; most cells were rounded up and detached from the substratum (Fig. 2 E). In contrast, the same treatment caused only a little damage to cells overexpressing NCS-1 (Fig. 2 F), indicating that the expression of NCS-1 rendered PC-12 cells more tolerant to H_2O_2 toxicity. The expression of NCS-1 reduced cell death caused by treatment with up to 1,000 μM H_2O_2 (Fig. 2 H). The aforementioned results were obtained from three cell lines transfected with NCS-1 and with corresponding vector-transfected control. A similar beneficial effect of NCS-1 on cell survival in response to 300 μM H_2O_2 was seen in two PC-12 cell lines that were not treated with NGF (not depicted).

NCS-1 promotes the long-term survival of primary cultured cortical neurons under stress and normal conditions

To further confirm the involvement of NCS-1 in neuronal survival, we overexpressed NCS-1 or its mutant E120Q in primary cultured embryonic rat cortical neurons that express endogenous NCS-1. The E120Q mutant possesses an amino acid substitution within the third EF-hand Ca^{2+}-binding motif, which impairs Ca^{2+} binding (Jeromin et al., 2004) but preserves the interaction with target proteins and, thereby, exerts a dominant-negative effect by disrupting the function of endogenous NCS-1 (Weiss et al., 2000). We used an adenoviral transfer system to transiently deliver the cDNA encoding NCS-1 together with EGFP (using an internal ribosome entry site–containing vector) and its E120Q mutant form into neurons cultured for 5 d in neurobasal medium containing B27 trophic supplements. As indicated by cells with EGFP fluorescence and nuclei stained with Hoechst 33258, nearly 70% of neurons were successfully infected with each virus at 3 d after infection (Fig. 3 A). We examined the effects of overexpression of wild-type and dominant-negative NCS-1 on neuronal survival under stress caused by B27 withdrawal, which has been reported to induce neuronal apoptosis (Brewer, 1995; Cheng et al., 2003). As shown in Fig. 3 B, B27 withdrawal promoted cell death in vector-treated control neurons (left; also compare the vector groups with and without B27 in Fig. 3 D). Overexpression of NCS-1, on the other hand, significantly rescued cells from death (Fig. 3 B, middle). In contrast, the expression of E120Q resulted in more severe cell death accompanying bleb formation (Fig. 3 B, right). To quantitatively analyze the time course for the changes in cell viability, the total number of surviving cells from the same field was counted daily by phase-contrast microscopy during 9 d (see Materials and methods). The results show that high cell viability was preserved upon expression of the wild-type NCS-1, whereas cell viability was reduced after the expression of E120Q; i.e., the number of days required to reach 70% cell viability were 5, 8, and 3 d for vector, NCS-1, and E120Q groups, respectively (Fig. 3 C). The expression levels of NCS-1 in each group of neurons before and after adenovirus infection in the absence of B27 trophic supplements are shown in the immunoblot (Fig. 3 E). Essentially the same results were obtained by counting neurons with condensed nuclei using

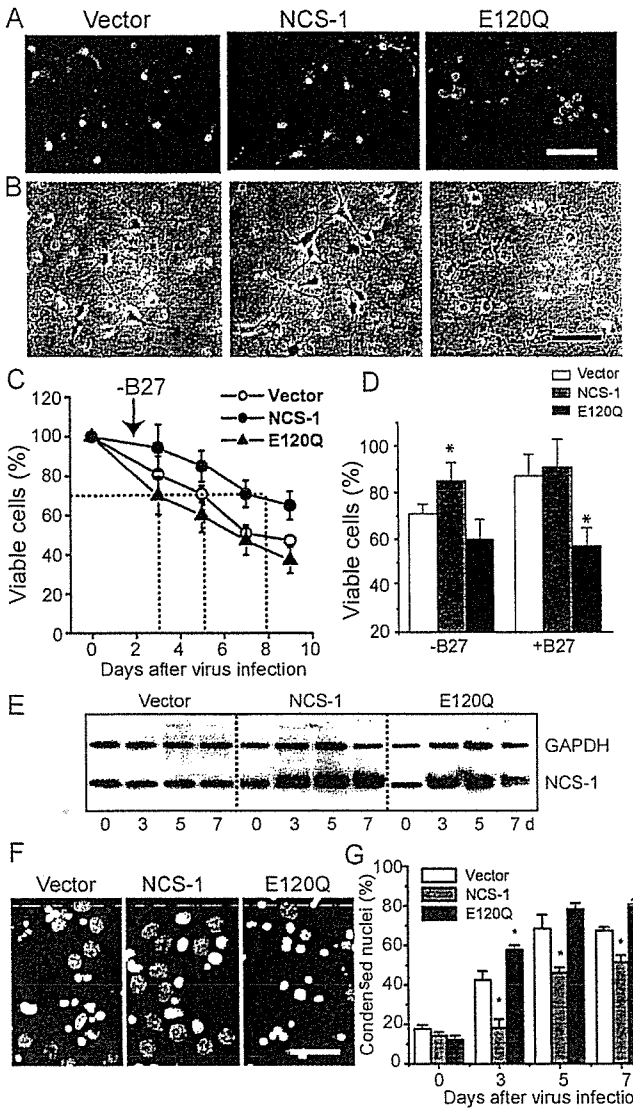

Figure 3. **Survival-promoting effect of NCS-1 in primary cultured cortical neurons.** Neurons were infected with adenovirus carrying EGFP vector alone, NCS-1, and its EF-hand mutant (E120Q) together with EGFP in the same internal ribosome entry site vector in culture medium containing neurobasal medium plus B27 trophic supplements, and they were further cultured in the presence or absence of B27 supplements (B27 supplements were withdrawn 2 d after the virus infections). (A) Fluorescent micrographs show the cultured neurons treated with adenovirus for 3 d (exhibiting strong EGFP signals) followed by treatment with a DNA-binding dye Hoechst 33258 to label their nuclei (red signals, pseudo-colored). (B) Phase-contrast micrographs show the cultured neurons treated with adenovirus for 5 d in the absence of B27 trophic supplements. Bars, 40 μm. (C) Time course of cell viability for neurons infected with adenovirus in the absence of B27 trophic supplements. Living neurons were counted daily by phase-contrast microscopy and plotted as a percentage of the initial number of neurons present on day 0 (n = 4). The number of days required to reach 70% cell viability is shown by the dotted lines. (D) Summary of cell viability data obtained from neurons cultured in the absence and presence of B27 trophic supplements at 5 d after virus infection. Error bars represent SEM. *, $P < 0.05$ versus the vector-controlled group. (E) Expression levels of NCS-1 and GAPDH in cultured neurons infected with each adenovirus indicated in the absence of B27 trophic supplements. (F and G) Staining patterns (light blue and white signals) of nuclei with Hoechst 33258 (F) and normalized numbers of cells having condensed nuclei (G). The dark blue color was changed to light blue or white to visualize signals more clearly. Bar, 15 μm.

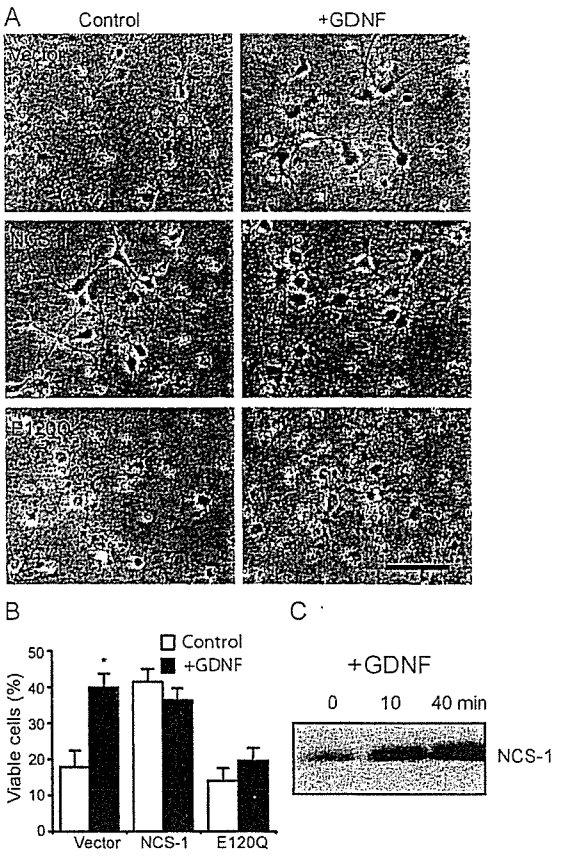

Figure 4. **NCS-1 mediates GDNF-induced neuronal survival.** (A) Primary cultured cortical neurons infected with adenovirus carrying vector alone (top), NCS-1 (middle), or E120Q mutant (bottom) were treated for 2 d with or without 10 ng/ml GDNF under the condition where B27 trophic supplement was depleted. Bar, 40 μm. (B) Summary of cell viability data. Viable cells were counted 2 d after GDNF treatment (+GDNF) or no treatment (control) and plotted as the percentage of the initial number of neurons present at day 0 in the same visual field (mean ± SEM [error bars]; n = 4). All neurons, not just transfected cells, were included in the cell viability counts. Note that treatment with E120Q largely prevented the GDNF-induced neuronal survival effect. *, $P < 0.05$ versus the data without exposure to GDNF. (C) Expression levels of NCS-1 in cultured neurons treated with 10 ng/ml GNDF for the indicated times.

Hoechst staining (Fig. 3, F and G), thus reinforcing the finding that the expression of NCS-1 protects neurons from cell death under apoptotic conditions. Furthermore, when B27 trophic supplement was kept in the culture medium (which is a less stress condition), the dominant-negative effect of E120Q was more clearly observed when compared with the vector control group (Fig. 3 D; also see A, where some blebs were observed in the neurons infected with E120Q mutant). In other preliminary experiments (not depicted), although the time course of the loss in cell viability was variable, overexpression of NCS-1 consistently delayed the loss of cell viability when B27 supplements were omitted, and the expression of E120Q always increased the rate of cell death when B27 was present. These results suggest that endogenous NCS-1 is playing an important role in keeping the long-term survival of cultured neurons under normal conditions in addition to the protective role from stress under apoptotic conditions.

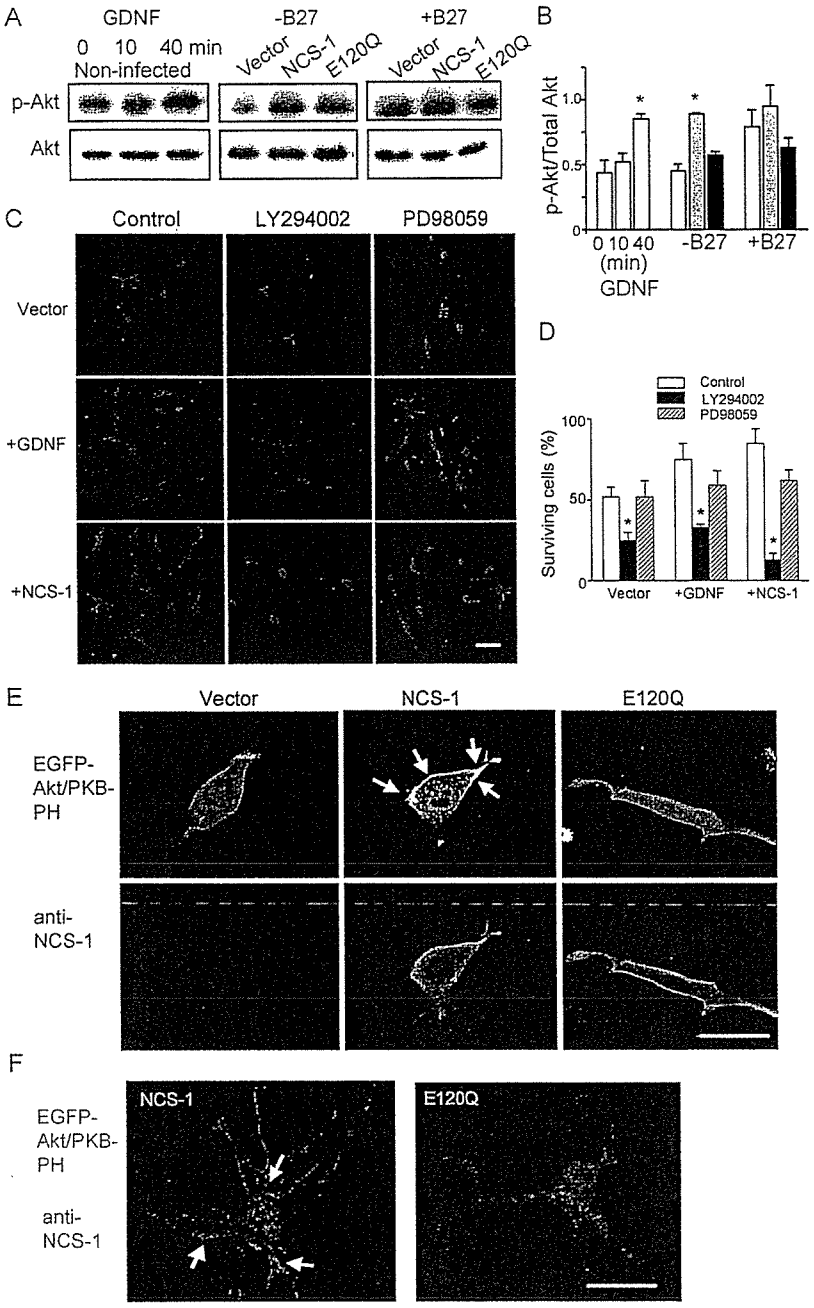

Figure 5. **NCS-1 promotes neuronal survival via activation of the PI3-K–Akt pathway.** (A and B) Both NCS-1 expression and GDNF treatment increase the phosphorylation of Akt kinase. Primary cultured cortical neurons were treated with 10 ng/ml GDNF for the indicated time periods or were infected with adenovirus carrying vector, NCS-1, or E120Q mutant and further incubated for 7 d in the presence or absence of B27 trophic supplements. They were then subjected to immunoblot analysis to detect protein levels of total (Akt) and phosphorylated form (p-Akt, the mixture of anti–P-Ser-473 and anti–P-Thr-308 antibodies, was used; A). The densities of phosphorylated Akt were normalized by those of total Akt levels and summarized in the bar graph (B). *, $P < 0.05$ versus vector control. (C and D) Both GDNF- and NCS-1–induced neuronal survival were abolished by PI3-K inhibitor but not by MEK inhibitor. Primary cultured cortical neurons were infected with adenovirus carrying NCS-1 or vector alone in medium lacking B27 trophic supplements. 3 d later, cultures were treated with 20 μM LY294002 or PD98059. For the vector-treated group, some cultures were further treated with 10 ng/ml GDNF. (C) Adenovirus-infected viable neurons treated or untreated with GDNF for 3 d. Bar, 40 μm. (D) Viable cells were counted and plotted as the percentage of the initial number of neurons present on day 0 (means ± SEM [error bars]; $n = 4$). *, $P < 0.05$ versus the data with no inhibitors. (E and F) NCS-1 activates Akt kinase by increasing the plasma membrane $PtdIns(3,4)P_2$ and $PtdIns(3,4,5)P_3$ levels in both CCL39 cells (E) and cultured neurons (F). CCL39 cells and primary cultured rat cortical neurons were transiently transfected with EGFP-Akt/PKB-PH together with either pCDNA3, NCS-1, or E120Q (1:3 ratios). 2 d later, cells were fixed, and immunocytochemistry was performed to detect NCS-1 proteins. Both EGFP distribution (E, top; and F, green signals) and NCS-1 expression (E, bottom; and F, red signals) were visualized using a laser confocal microscope. Laser confocal sections through the middle of representative cells in each treatment are shown. Arrows indicate the peripheral redistribution of the EGFP–PKB–PH in NCS-1–expressing cells. Bars, 10 μm.

NCS-1 mediates GDNF-induced cell survival

A large body of evidence suggests that neuronal survival is promoted by neurotrophic factors such as BDNF and GDNF (Boyd and Gordon, 2003). Because the long-term application of GDNF has been reported to enhance the expression of NCS-1 in *Xenopus laevis* motor neurons (Wang et al., 2001), we attempted to clarify the role of NCS-1 as a downstream mechanism of GDNF-induced cell survival in rat cortical neurons. When primary cultured cortical neurons were treated with 10 ng/ml GDNF for 2 d after the withdrawal of B27 supplements, neuronal survival was significantly enhanced when compared with time-matched control (Fig. 4, A [top] and B). Interestingly, the expression of NCS-1 mimicked the survival-promoting effects of GDNF; i.e., NCS-1 exerted a robust survival effect even in the absence of GDNF (Fig. 4, A [middle] and B). Most strikingly, the expression of the dominant-negative NCS-1 mutant E120Q largely prevented cell survival induced by GDNF (Fig. 4, A [bottom] and B). Immunoblot analysis revealed that the application of 10 ng/ml GDNF resulted in a significant increase in the expression level of endogenous NCS-1 within 10 min, which further increased at 40 min in these neurons (Fig. 4 C). The amount of NCS-1 remained elevated through 2 d of exposure to GDNF (not depicted). These results show that the treatment of GDNF increases the expression level of NCS-1, which subsequently promotes neuronal survival, suggesting that GDNF-induced neuroprotection is at least in part mediated by NCS-1.

Activation of the PI3-K-Akt pathway is involved in NCS-1-induced neuronal survival

In neurons, GDNF has been reported to promote cell survival via activation of signaling cascades involving the PI3-K–Akt pathway (Soler et al., 1999; Takahashi, 2001). In accordance with these studies, we also observed that exposure of primary cultured cortical neurons to GDNF resulted in a large increase in phospho-Akt levels (Fig. 5 A, left). Therefore, it was of interest for us to test whether NCS-1 also activates this kinase. We examined the effect of NCS-1 expression or its dominant-negative form on Akt phosphorylation in the presence or absence of B27 trophic supplements. When B27 trophic supplements were absent, the expression of NCS-1 significantly enhanced the phosphorylation of Akt, whereas expression of the dominant-negative mutant E120Q had little effect when compared with control vector-infected neurons (Fig. 5, A [middle] and B). On the other hand, when B27 supplements were present, a relatively high level of phosphorylated Akt was observed in the vector-treated control group (Fig. 5, A [right] and B). Additional expression of exogenous NCS-1 further increased the Akt phosphorylation level, whereas expression of the dominant-negative mutant suppressed phosphorylation (Fig. 5, A [right] and B). Thus, the phosphorylation levels of Akt in each group of neurons were well correlated with their viabilities, as shown in Fig. 3 D.

In addition, pretreatment of cultured cortical neurons with LY294002, an inhibitor of PI3-K, completely abolished both GDNF- and NCS-1–induced neuronal survival, whereas PD98059, an inhibitor of MAPK kinase (MEK), did not (Fig. 5, C and D). These results suggest that the NCS-1–induced survival-promoting effect is mediated via the PI3-K–Akt pathway but not the MAPK pathway in cultured cortical neurons.

To further understand the upstream mechanism of the NCS-1–induced activation of Akt, we next examined the effect of overexpression of NCS-1 and E120Q on the subcellular localization of Akt/PKB in living cells. Akt/PKB is known to be translocated to the plasma membrane when it is fully activated upon phosphorylation and bound with its substrates PtdIns(3,4)P_2 and PtdIns(3,4,5)P_3 (Alessi et al., 1996). We constructed the GFP-tagged pleckstrin homology (PH) domain of Akt/PKBα (EGFP-Akt/PKB-PH) and transiently cotransfected it into CCL39 cells, which express a small amount of endogenous NCS-1, together with NCS-1, E120Q, or empty vector. 2 d later, the subcellular localization of EGFP-tagged Akt/PKB-PH was assessed on a confocal microscope. Akt/PKB-PH was diffusely localized in the cytosol of vector-transfected control cells (Fig. 5 E). Interestingly, Akt/PKB-PH became localized in the peripheral region of cells when NCS-1 was coexpressed, but this peripheral localization was abolished when E120Q was coexpressed (Fig. 5 E). Qualitatively similar results were also obtained when primary cultured cortical neurons were treated with the same vectors; i.e., Akt/PKB-PH was localized in the peripheral regions of neurons when NCS-1 was overexpressed, but a more diffuse localization pattern was observed when E120Q was overexpressed (Fig. 5 F). The distribution pattern of Akt/PKB-PH in vector-transfected neurons was similar to that of NCS-1–overexpressing cells (not depicted). These results strongly demonstrate that NCS-1 increases the levels of plasma membrane PtdIns(3,4)P_2 and PtdIns(3,4,5)P_3 and, thus, activates Akt/PKB in living cells.

Dominant-negative NCS-1 accelerates the in vivo axotomy-induced loss of neurons

We examined the effects of the overexpression of NCS-1 and its dominant-negative mutant on the survival of these neurons to clarify the physiological role of NCS-1 in injured motor neurons in vivo. One side of vagus nerves of adult rats were axotomized as previously described (Fig. 1) and infected with adenoviral vectors encoding NCS-1, E120Q, or EGFP vector alone, and neuronal degeneration was evaluated by histological analysis. 1 wk after axotomy, nearly 30% of nerve cells were found to be EGFP positive in the injured side (Fig. 6 A). There were clear differences in the staining pattern between control and injured sides for all groups, probably because the regeneration process, such as activation of the surrounding glial cells, was ongoing on injured sides. However, the number of surviving motor neurons stained with hematoxylin were not significantly decreased at the injured side for vector-treated DMV sections (Fig. 6, B and D; examples of counted neurons are indicated by black arrows in C). This would probably be the result of natural antiapoptotic mechanisms induced by injury, which exist in mature neurons as previously reported (Benn and Woolf, 2004). Because the expression level of NCS-1 was significantly increased in response to in vivo axotomy (Fig. 1), we hypothesized that NCS-1 may be involved in this antiapoptotic mechanism. If so, blocking of endogenous NCS-1 would reduce this beneficial effect. As expected, the dominant-negative E120Q mutant resulted in a significant loss of neurons in the injured side (Fig. 6, B–D), and some TUNEL-positive nuclei were also detected only in this group (Fig. 6 E, arrows; and its magnified image in F). Considering that the infection efficiency was only ~30% in these experiments, a large majority of neurons successfully infected with E120Q appear to have undergone apoptosis. Infection of neurons with the functional NCS-1 adenovirus only had a modest effect on neuronal survival. This probably results from both the low infection efficiency and the high levels of endogenous NCS-1 expression in axotomized neurons (Fig. 1) because the NCS-1 effects are already close to maximum. Thus, the dominant-negative mutant E120Q inhibited the survival of adult DMV neurons from axotomy-induced injury, strongly suggesting that NCS-1 is one of the important factors mediating neuronal survival after in vivo axotomy.

Discussion

Numerous stressors, including physical or chemical injury and genetic abnormalities, lead to neuronal degeneration by programmed cell death along an apoptotic pathway. Under these conditions, some intrinsic and extrinsic factors, including neurotrophic factors, are known to activate the antiapoptotic process to rescue neurons from death. However, the signaling pathway leading to cell survival is not yet completely understood.

In this study, we identified a novel function for the Ca^{2+}-binding protein NCS-1, which (1) promotes the long-term survival

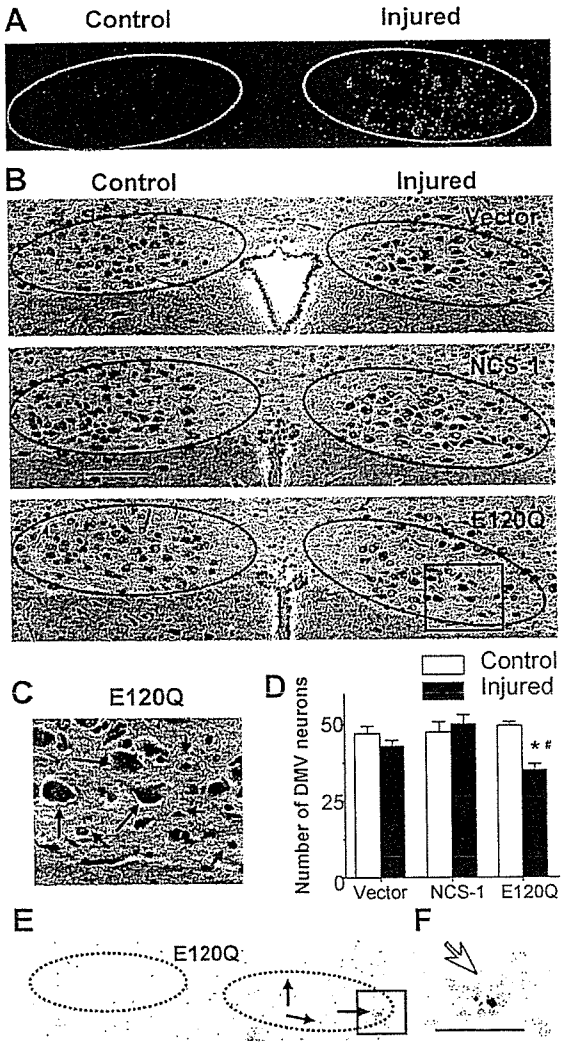

Figure 6. **Dominant-negative NCS-1 mutant E120Q promotes the axotomy-induced degeneration of DMV neurons.** After the axotomy of vagus motor neurons were performed as described in Fig. 1, adenoviral vectors carrying NCS-1, E120Q, or EGFP alone were injected from the stump of the nerve. 1 wk after the treatment, the brainstem was excised, and serial sections were cut. (A) Representative EGFP fluorescence image showing that EGFP signals were detected in some cells on the injured side. Positions of DMV neurons are indicated by circles in A, B, and E. (B) Histological evaluation of DMV neurons in adenovirus-treated animals by hematoxylin/eosin staining. (C) Magnified image of the boxed area in B for E120Q-treated DMV neurons. Only neurons (indicated by black arrows), not nuclei, of glial or endothelial cells (indicated by red arrows) were counted. (D) Summarized data obtained from B. *, $P < 0.05$ versus the control side of the same section. #, $P < 0.05$ versus the injured side of vector-treated animals (means ± SEM [error bars]; $n = 6$ from three animals). (E) An example of the TUNEL-staining pattern obtained from an E120Q-treated animal. (F) The magnified image of the boxed area in E. TUNEL-positive nuclei are indicated by arrows. Bar (B), 100 μm; (F) 25 μm.

of cultured neurons via PI3-K–Akt signaling pathways; (2) mediates, at least in part, GDNF-induced neuroprotection; and (3) is up-regulated in response to axonal injury and plays an important role in the antiapoptotic mechanism in injured motor neurons.

NCS-1 is a novel survival-promoting factor in neuronal cells

We observed that the overexpression of NCS-1 rendered PC-12 cells and primary cultured cortical neurons more tolerant to several kinds of stressors, such as oxidative stress or trophic supplement withdrawal (Figs. 2 and 3), demonstrating that the expression of NCS-1 protects neurons from cell death under apoptotic conditions. In addition, overexpression of an EF-hand dominant-negative mutant E120Q significantly accelerated apoptosis when B27 trophic supplements were kept in the culture medium (Fig. 3 D), suggesting that endogenous NCS-1 is important for keeping the long-term survival of cultured neurons under normal (or less apoptotic) conditions. The latter finding also indicates that Ca^{2+} binding is required for NCS-1–mediated cell survival. On the basis of these findings, we propose that NCS-1 is a novel member of survival-promoting factors in cultured neurons.

NCS-1 mediates GDNF-induced cell survival via activation of the PI3-K-Akt survival pathway

We found that treatment of cultured cortical neurons with a neurotrophic factor GDNF increased the expression level of NCS-1 (Fig. 4 C) and enhanced neuronal survival (Fig. 4, A and B), which is consistent with a previous study reporting that GDNF enhanced the expression of frequenin/NCS-1 in *Xenopus* motor neurons (Wang et al., 2001). GDNF-induced increase in the NCS-1 level appeared to be caused by the synthesis of protein and/or mRNA but not by the prevention of NCS-1 degradation because GDNF did not raise the expression level of NCS-1 in the presence of the inhibitor of protein synthesis cycloheximide (10 μg/ml for 20 h; not depicted). In contrast to the vector-treated control neurons, GDNF did not further enhance the survival effect in neurons overexpressing NCS-1 (Fig. 4, A and B), suggesting that cell viability was already sufficiently high under this condition. Strikingly, the survival-promoting effect of GDNF was largely prevented by overexpression of the dominant-negative mutant E120Q (Fig. 4, A and B), suggesting that NCS-1 mediates the GDNF survival signal.

GDNF activates at least two intracellular pathways in neurons: one involving the PI3-K–Akt pathway and another involving the MAPK (p42 and p44, also called ERK1 and ERK2) pathway. However, PI3-K but not the MAPK pathway has been reported to be responsible for GDNF-mediated neuronal survival in motor neurons (Soler et al., 1999). In accordance with this study, we observed that exposure of primary cultured cortical neurons to GDNF resulted in a large increase in the phospho-Akt level (Fig. 5 A). In the same way, the overexpression of NCS-1 also dramatically enhanced the phosphorylation levels of Akt both in the presence and absence of B27 trophic supplements, whereas the overexpression of dominant-negative mutant E120Q did not (Fig. 5 A). In addition, the NCS-1–nduced survival-promoting effect was largely inhibited by the PI3-K inhibitor LY294002 but not the MEK inhibitor PD98059 (Fig. 5, C and D). Furthermore, NCS-1 increased the plasma membrane $PtdIns(3,4)P_2$ and $PtdIns(3,4,5)P_3$ levels, which indicates the activation of Akt in intact cells (Fig. 5, E and F). These results strongly suggest that NCS-1 is a novel downstream target that mediates GDNF survival signal through activation of the PI3-K–Akt pathway.

Possible mechanisms of the action of NCS-1

Several possible mechanisms may underlie the survival action of NCS-1. We observed that Akt/PKB-PH was recruited to the plasma membrane when NCS-1 was coexpressed, suggesting that NCS-1 acts upstream of the Akt pathway. NCS-1 was previously reported to activate PI4-K (Hendricks et al., 1999), which increases the level of plasma membrane PtdIns(4)P, the substrate of PI3-K, as well as PI5-K. Therefore, upon activation of these kinases, other phosphoinositides would be produced. Indeed, it has been reported that the overexpression of NCS-1 significantly increased both PtdIns(4)P and PtdIns(4,5)P_2 levels in PC-12 cells (Koizumi et al., 2002). Furthermore, PtdIns(3,4)P_2 and PtdIns(3,4,5)P_3, the substrates of Akt/PKB, would also be produced, which, in turn, would activate the Akt pathway (Cantley, 2002). As expected, the overexpression of NCS-1 increased the plasma membrane PtdIns(3,4)P_2 and PtdIns(3,4,5)P_3 levels both in CCL39 cells and neuronal cells (Fig. 5, E and F), enhanced the phosphorylation of Akt (Fig. 5 A), and promoted neuronal survival (Fig. 3). Therefore, we propose that activation of such a phosphatidylinositol pathway is a mechanism for the survival action of NCS-1. In addition, we observed that in contrast to GDNF, our preliminary data show that BDNF did not increase the expression level of NCS-1 (unpublished data) despite the reported survival-promoting effect of BDNF in cultured cortical neurons (Cheng et al., 2003). Interestingly, BDNF-induced survival signaling has been reported to be mediated by CaM, another Ca^{2+}-binding protein in cortical neurons (Cheng et al., 2003), and CaM has been reported to directly activate PI3-K (Perez-Garcia et al., 2004). Therefore, NCS-1 mediates the GDNF signal by activating PI4-K, whereas CaM mediates the BDNF signal by activating PI3-K. These two signals would lead the survival signal to the Akt pathway.

On the other hand, it is also possible that NCS-1 promotes neuronal survival by some other mechanisms in addition to activation of the Akt pathway. For example, the survival-promoting effect of NCS-1 appears to be analogous to that of the recently characterized antiapoptotic protein family called inhibitors of apoptosis, which suppress apoptosis through the direct inhibition of caspases (Liston et al., 2003). Some of these proteins, such as neuronal apoptosis inhibitory protein and X-linked inhibitors of apoptosis protein, have been reported to be essential for GDNF-mediated neuroprotective effects in injured motor neurons in vivo (Perrelet et al., 2002). Furthermore, recent evidence demonstrates that neuronal apoptosis inhibitory protein interacts with hippocalcin, another closely related Ca^{2+}-binding protein that affects caspase-12 activity (Korhonen et al., 2005) and protects neurons against Ca^{2+}-induced cell death (Mercer et al., 2000). Therefore, we do not exclude the possibility that like these proteins, NCS-1 also exerts a more direct effect on some caspases. We are currently investigating the possible interaction of these proteins.

As NCS-1 is known to interact with voltage-gated K^+ channels (Kv4; Nakamura et al., 2001), it might also increase the resistance of neurons to excitotoxic apoptosis through the activation of K^+ channels. Increased outward K^+ current would prevent neurons from reaching firing threshold and, thereby, prevent cells from Ca^{2+} overload leading to cell death.

NCS-1 is a novel survival-promoting factor up-regulated in injured neurons

In this study, we found that the expression level of NCS-1 was significantly increased in response to axonal injuries (transection of the vagus nerve as well as treatment of nerves with colchicine) in the DMV neurons of adult rats (Fig. 1). The behavior of NCS-1 appears to be analogous to that of the recently identified protein damage-induced neuronal endopeptidase, which is expressed in response to neuronal damages induced by nerve transection and colchicine treatment in both the central and peripheral nervous systems (Kiryu-Seo et al., 2000). Because antiapoptotic mechanisms are activated in mature neurons in response to stress to protect against accidental apoptotic cell death, it has been described that peripheral axotomy in adult neurons does not result in extensive cell death (Benn and Woolf, 2004). In accordance with this, we also observed that little loss of motor neurons was evident by in vivo axotomy in vector-treated control neurons (Fig. 6, B and D). The expression of exogenous NCS-1 did not exert the further beneficial effect (Fig. 6, B and D). This marginal effect of exogenous NCS-1 (compared with the vector control group) would be the result of the increased expression level of endogenous NCS-1 in axotomized neurons, which occurs for all groups. In contrast, overexpression of dominant-negative E120Q significantly decreased the number of surviving neurons (Fig. 6, B–D) and produced TUNEL-positive apoptotic neurons at the injured side (Fig. 6, E and F), indicating that disruption of NCS-1 function increased the vulnerability of DMV neurons to axotomy.

Overexpression of NCS-1 rendered PC-12 cells resistant to H_2O_2 toxicity even in the absence of GDNF (Fig. 2), suggesting that NCS-1 itself is enough to promote cell survival. This is consistent with our view that NCS-1 is the downstream target for GDNF. Because growing evidence indicates that nerve injury leads to the up-regulation of multiple antiapoptotic molecules, including GDNF (Liberatore et al., 1997; Yamamoto et al., 1998; Wang et al., 2002), it is possible that neuronal damages induced by in vivo axotomy enhance the synthesis and/or secretion of GDNF, which, in turn, up-regulates NCS-1 expression and promotes neuronal survival in injured neurons. Although an underlying mechanism would be different, the up-regulation of NCS-1 has also been reported in the cortex of schizophrenic and bipolar patients, demonstrating the involvement of NCS-1 in neurological disease (Koh et al., 2003).

In conclusion, we characterized a novel function of NCS-1 mediating a GDNF-induced neuroprotective effect via activations of Akt kinase. Furthermore, we found that NCS-1 is up-regulated in response to nerve injury and plays an important role in the antiapoptotic mechanism in adult motor neurons. Our present findings would provide new and basic insights into the mechanism of neuronal regeneration.

Materials and methods

Plasmids and viral vectors

E120Q NCS-1 point mutant was generated with a conventional PCR protocol using the wild-type rat NCS-1 (GenBank/EMBL/DDBJ accession no. L27421 as a template and was sequenced to confirm the mutation.

Akt/PKBα cDNA was cloned from the human kidney cDNA library (CLONTECH Laboratories, Inc.), and NH_2-terminally tagged fluorescent protein EGFP-Akt/PKB-PH was constructed incorporating a fragment of 750 bp, encoding the first 250 amino acids of PKBα (containing the PH domain) into EGFP-vector as described previously (Currie et al., 1999).

Adenovirus containing wild-type NCS-1 and the E120Q mutant inserts were generated by cotransfecting either of these plasmids and pBHG11 (Microbix Biosystems, Inc.) into HEK 293 cells. Viral DNA was isolated from the supernatant in the wells displaying the cytopathic effect. Replication-incompetent virus containing DNA inserts were plaque-purified twice and grown on HEK 293 cells to produce large amounts of adenovirus. Tissue culture supernatant containing adenovirus was concentrated by centrifugation over cesium chloride. The titers of viral stocks were 2.2×10^{10} pfu/ml for EGFP–NCS-1, 1.1×10^{10} pfu/ml for EGFP-E120Q, and 2.2×10^{10} pfu/ml for EGFP-vector.

Cell cultures

PC-12 cells stably transfected with vector alone or vector containing cDNA coding for the wild-type NCS-1 (several clones) were grown onto collagen-coated (500 μg/ml of type I; Sigma-Aldrich) culture dishes in growth medium (DME containing 10% horse serum, 5% FBS, and 400 μg/ml geneticin and gentamicin) as described previously (Koizumi et al., 2002). When cells became 80% confluent, they were switched to the differentiation medium (growth medium with half serum) supplemented with 100 ng/ml NGF-7S (Invitrogen).

Primary culture of cortical neurons was performed using the cortex from Sprague-Dawley rats at embryonic day 18. In brief, cortical tissues were isolated from whole brain, minced into small pieces, and digested for 10 min at 37°C in a 20-U/ml papain solution containing 0.002% DNase I (Worthington Biochemical Corp.). After titration of the enzymatic activity, cells were mechanically dissociated by several passages through pipette tips. After centrifugation, cells were resuspended in neurobasal medium supplemented with B27 trophic factors (both from Invitrogen), whose compositions were reported previously (Brewer et al., 1993). They were then plated onto culture dishes coated with 0.1% polyethylenimine at a density of $2.5–5 \times 10^4$ cells/cm^2 for cell survival assay and 10^5 cells/cm^2 for immunoblot analysis.

Fluorescent microscopy

CCL39 cells and primary cultured rat cortical neurons were plated onto collagen-coated glass coverslips and cultivated for 1 d. They were then transiently transfected with the EGFP-Akt/PKB-PH construct together with either NCS-1, E120Q, or pCDNA3 (1:3 ratio) using LipofectAMINE 2000 (Invitrogen) and were subjected to immunocytochemistry. In brief, cells were fixed with 4% PFA, permeabilized with 0.2% Triton X-100, and blocked with 5% BSA. They were then incubated for 1 h with anti–NCS-1 antibody (1:200) followed by incubation with secondary antibodies (FITC- or rhodamine-conjugated goat anti–rabbit IgG; 1:200; Jackson ImmunoResearch Laboratories). After extensive wash with PBS, cell images were scanned on a laser confocal microscope (MRC-1024K; Bio-Rad Laboratories) or obtained with conventional epifluorescence illumination (BX50WI; Olympus) with a cooled CCD camera (CoolSNAP; Photometrics) using a 0.9-W 60× water immersion objective lens. Immunocytochemistry for PC-12 cells were also performed in the same way.

Evaluation of neuronal survival

The primary cultured neurons were infected with viruses at a multiplicity of infection of 100 pfu/cell at 5 d after plating. Under this condition, we found that nearly 70% of the neurons were infected by monitoring EGFP fluorescence (Fig. 3 A). The number of living neurons was counted within the fixed area of images taken by a digital camera (Coolpix 4500; Nikon). To count the number of cells always within the same area, a grid seal with numbering (Asahi Techno glass) was stuck on the bottom of each culture dish. The number of living neurons remaining at each day was expressed as a percentage of the initial number. Neurons showing the degenerating stage characterized by nuclear condensation, membrane blebbing, or extensive neurite fragmentation were excluded. Four different regions were selected from one dish, and six separate experiments were performed for each condition.

To identify and quantify apoptotic neurons, cells were fixed with 4% PFA and were stained with Hoechst 33258. Coverslips were mounted onto glass slides, and cells were observed under epifluorescence illumination on an inverted microscope (1X71; Olympus) using a 40× NA 1.35 oil immersion objective lens (Olympus). Cells were considered apoptotic if their nuclear chromatin was condensed or fragmented, whereas cells were considered viable if their chromatin was diffusely and evenly distributed throughout the nucleus (Fig. 3 F).

Immunoblot analysis

DMV tissue samples were obtained by scratching the DMV neurons from several frozen sections of brainstem (described in the next section) using pulled glass capillary under the light microscope. These tissue samples or cultured cells (PC-12 cells and cortical neurons) were then solubilized in SDS-PAGE sample buffer containing protease and phosphatase inhibitors and subjected to immunoblot analysis using image density software (Scion Image; Scion Corp.) as previously described (Nakamura et al., 2001). Primary antibodies used were anti–NCS-1 antibody (1:1,000), which was previously described (Jeromin et al., 1999), and publicly available antibodies: monoclonal anti-GAPDH antibody (1:1,000) obtained from Chemicon as well as antiphospho-Akt antibodies (detectable for the phosphorylation of Thr308 and Ser473; 1:1,000) and anti-Akt antibody (1:1,000; both from Cell Signaling Technology). Secondary antibodies used were HRP-conjugated anti–rabbit and anti–mouse antibodies or a combination of biotinylated anti–rabbit (or mouse) antibodies (Zymed Laboratories) and HRP-conjugated streptavidin (Zymed Laboratories).

In vivo axotomy and colchicine treatment

The method of vagus axotomy was described previously (Nabekura et al., 2002a). In brief, 4–6-wk-old Sprague-Dawley rats were deeply anesthetized with 50 mg/kg pentobarbital, and axotomy of the vagus motor neurons was performed with fine scissors at the unilateral vagus nerve at the neck. Injured neurons were confirmed by detecting the fluorescence of Di-I in the DMV, which had been placed at the proximal cut site of the nerve bundle (Nabekura et al., 2002a).

To test the effects of colchicine, an implantable polymer containing 10% (wt/vol) colchicine was made by mixing colchicine with ethylene-vinyl acetate copolymer (Elvax) followed by drying as described previously (Kakizawa et al., 2000). Solid slices (~1 mm^2) were placed around the unilateral vagal nerve to allow the continuous release of colchicine from slices. The skin incision was closed, and rats were returned to the cage after awaking from the anesthetic.

Histology

1 d to 2 mo (usually 1 wk) after receiving ipsilateral vagal axotomy, brainstems were quickly removed, and 8–10-μm-thick frozen sections were cut. Immunohistochemistry was performed using the labeled biotin–streptavidin method. In brief, after fixation and blocking, the sections were incubated at 4°C overnight with a rabbit polyclonal antibody against NCS-1 at a dilution of 1:15,000 and were sequentially incubated with a biotinylated anti–rabbit secondary antibody and a HRP-conjugated streptavidin–biotin complex (GE Healthcare). The colored reaction product was developed with DAB solution. The sections were lightly counterstained with hematoxylin to visualize nuclei. Images were acquired using a digital camera (FX380; Olympus) equipped with an image filing software (FLVFS-LS; Flovel).

Comparison of the expression level of NCS-1 between injured and control sides were performed using computerized image analysis (Win Roof; Mitani Corp.). In brief, the DMV region from the injured side was at first selected, and the image was converted to binary images by thresholding so that only the area highly stained with anti–NCS-1 antibody could be detected. The same threshold level was used for both the control and injured DMV in each tissue section. The highly stained area was summated and represented as normalized values.

Neuronal degeneration was evaluated by counting surviving neurons as described previously (Rothstein et al., 2005) as well as by TUNEL staining using the apoptag peroxidase in situ Apoptosis Detection Kit (Chemicon). In brief, in vivo axotomy was performed as described above, and, at the same time, adenoviral vectors carrying EGFP only, EGFP plus NCS-1, or E120Q (10^9 pfu each) was injected into the stump of the nerve using a 34-gauge needle. 1 wk after axotomy, paraffin-embedded serial sections (3–4 μm) were made from the brainstem. After they were deparaffinized, sections were directly stained with hematoxylin/eosin to visualize the structure of the DMV region. TUNEL staining was performed in accordance with the manufacturer's method. The sections were lightly counterstained with methyl green. Control sections were treated similarly but incubated in the absence of TdT enzyme. To confirm whether the adenoviral vectors were transferred to the DMV neurons, another set of animals were treated in the same way. 8-μm frozen sections were cut 1 wk after operation, and EGFP signals were viewed under a fluorescence microscope (1X71; Olympus). All image acquisitions were performed at room temperature, and images were subsequently processed using Adobe Photoshop (version 7) and Adobe Illustrator (version 10) software. All experiments conformed to the Guiding Principles for the Care and Use of Animals approved by the Council of the Physiological Society of Japan. All efforts were made to minimize the number of animals used and their suffering.